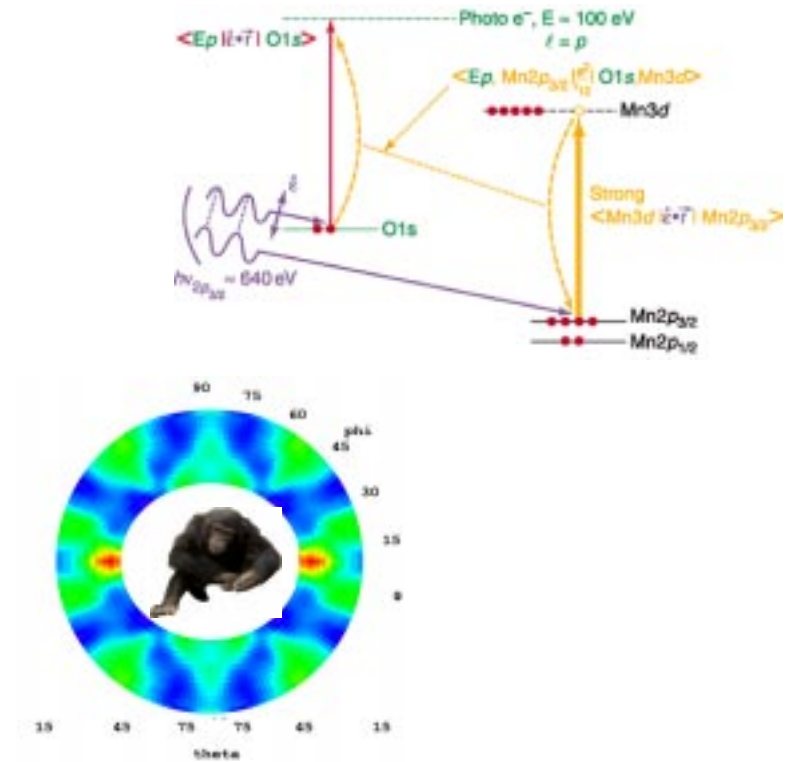
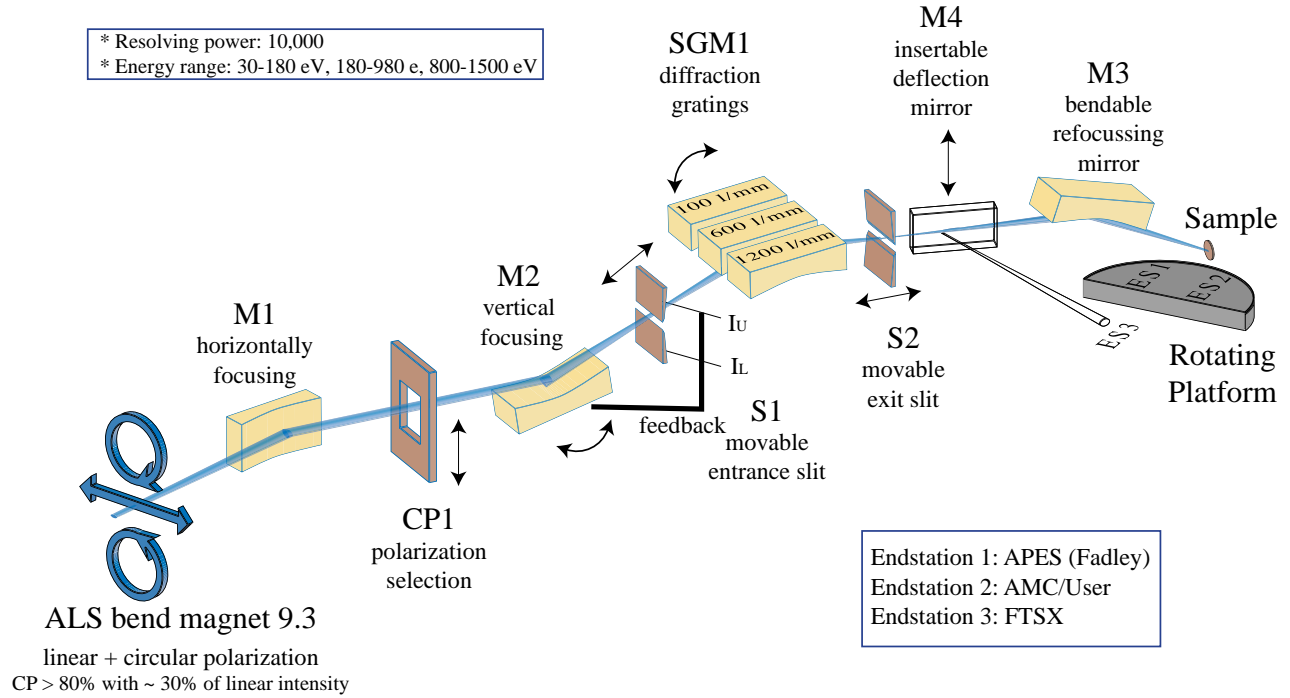


Beamline 9.3.2

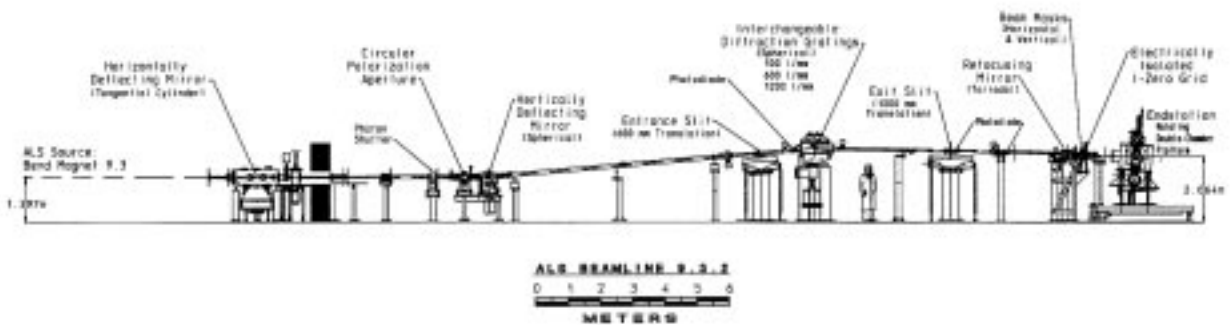
Operations and Components



ALS Beamline 9.3.2



E. J. Moler 9/98



Prepared by Edward J. Moler, 1999

Contents

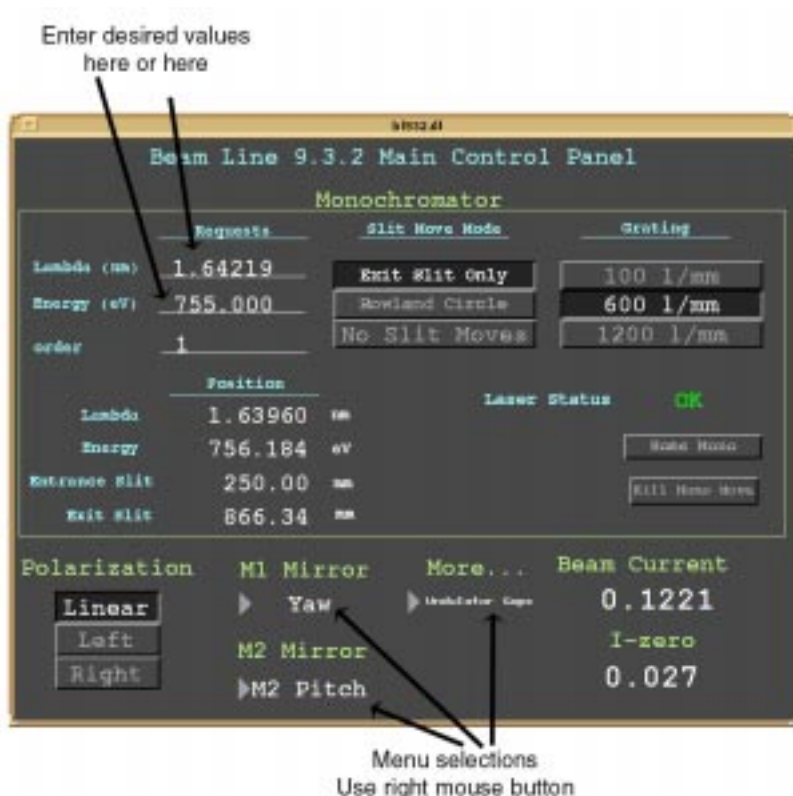
Introduction	4
The beamline user controls.....	4
Selecting the monochromator resolving power	5
Selecting gratings.....	6
Selecting photon polarization	7
Selecting the slit movement mode	7
Opening the beamline to the ring and to the endstations ..	8
Connecting a user endstation	8
Getting the beam into the endstation	9
Optimising the M2 feedback loop.....	9
Booting the beamline from scratch	10
Calibrating the Photon Energy.....	12
Caveats and Known Problems	12
Other Technical Details	13
<i>Directories and files of the user interface</i>	<i>13</i>
<i>VME crate and code</i>	<i>13</i>
<i>Endstation Interface to monochromator control system</i>	<i>13</i>
<i>Optics</i>	<i>13</i>

Introduction

This document describes the components and operations of beamline 9.3.2. It supercedes the information originally appearing in Light Source Note LSBL-336.

The beamline user controls

To operate the beamline, one must first logon to the display server and start the user interface. The user interface is designed to allow all typical actions to be accessed from a single window. Important error conditions are also displayed in this window. The interface



is written in the EPICS display-manager package.

- ▶ Logon to the SUN workstation bl93-102.als.lbl.gov with an X-window program or sitting directly at the console. Contact a beamline representative for username and password.
- ▶ Type 'show' at an X-terminal prompt [If you are using the SUN in the sector 10 facilities-rack, type 'show10']. The beamline 9.3.2 main control panel should appear within a few seconds.

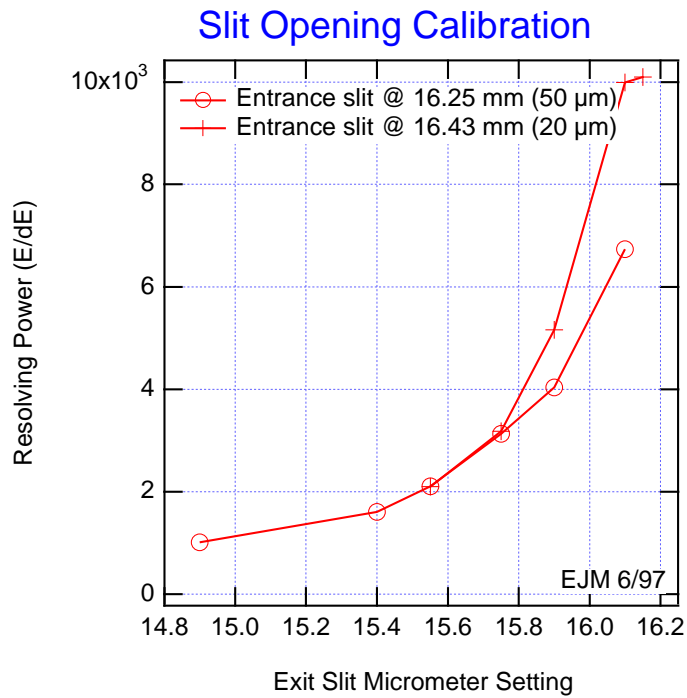
The main control panel allows the user to select a photon energy or wavelength.

- ▶ Position the cursor over the energy or wavelength field in the main control panel.
- ▶ Edit the number to select the desired value.
- ▶ Either hit return or move the cursor out of the field. The grating and slits will move to the appropriate place as indicated by the units of the position displays turning green. When all components are in position, all units labels will return to white.

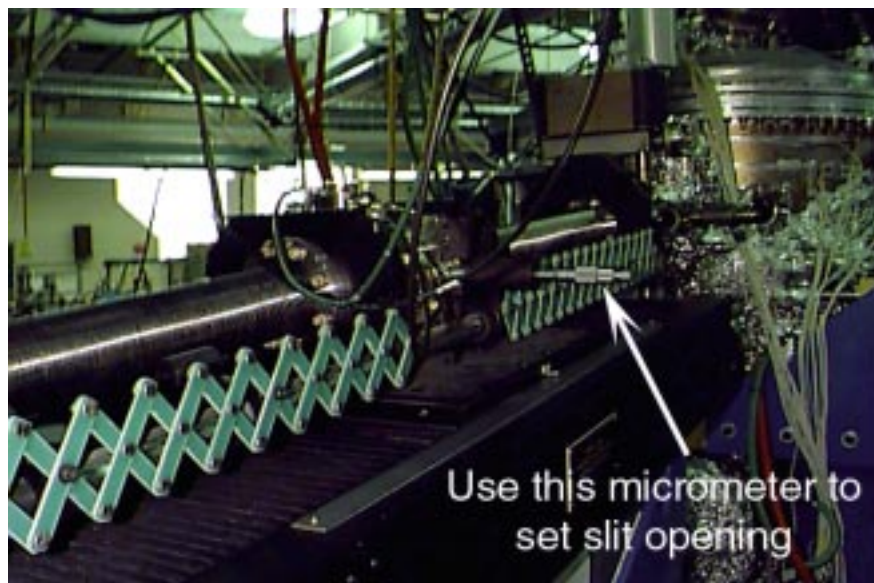
Selecting the monochromator resolving power

The resolution of the monochromator is set by adjusting the exit slit opening. The entrance slit is left at a fixed opening for most experiments, but may also be adjusted for the extremes of highest resolution or highest flux.

- ▶ Choose the resolving power desired and read the micrometer settings required using the graph.
- ▶ Adjust the micrometers on the exit and entrance slit to the desired values.

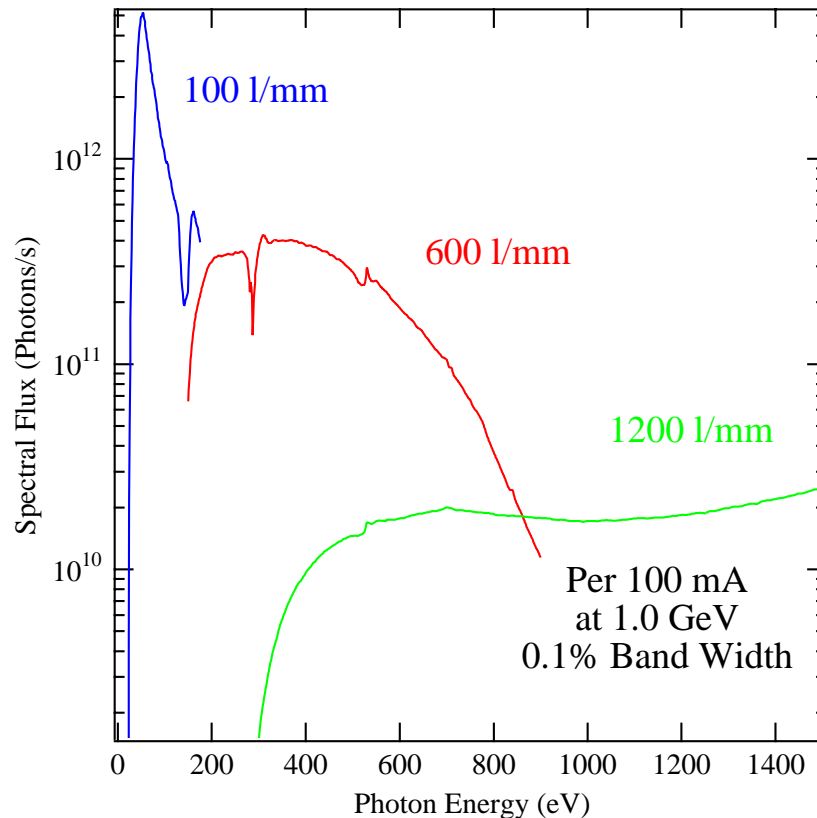


Entrance Slit



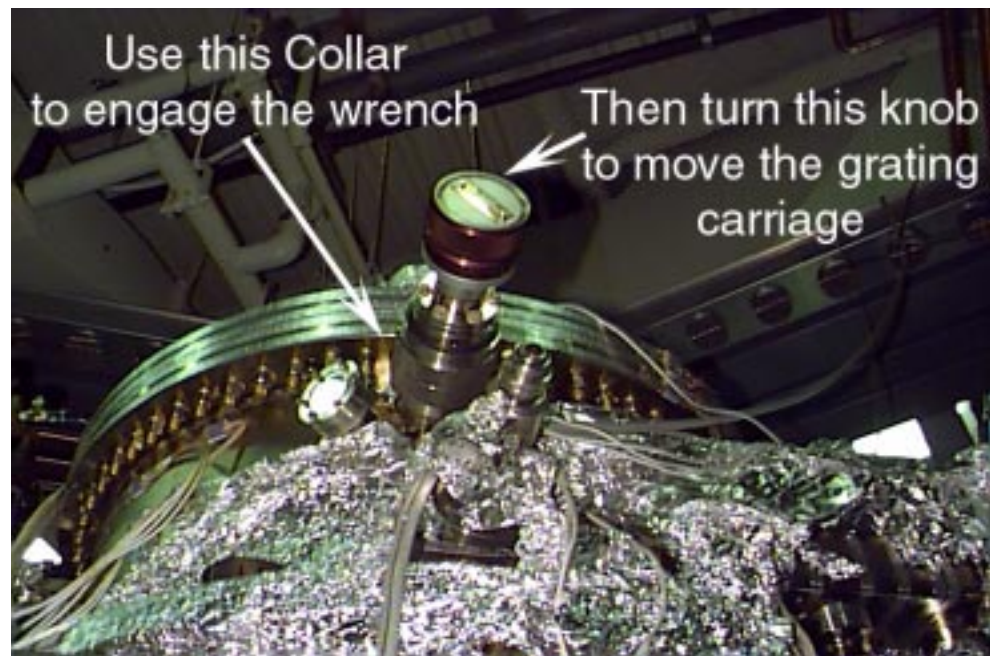
Selecting gratings

The monochromator allows in-situ switching of three gratings. Each grating covers different energy ranges with varying efficiencies. The grating is changed using an allen wrench to move the grating carriage. The allen wrench is mounted on a rotary feedthrough with a linear motion drive to engage the wrench.



- ▶ Select which grating is desired using the graph of flux vs. photon energy.
- ▶ Set the grating position to align with the allen wrench. Do this by setting the photon energy to 65 eV for the 100 l/mm grating or 450 eV for the 600 l/mm grating.
- ▶ Insert the wrench by turning the linear-motion collar until the wrench firmly engages the lead-screw socket.
- ▶ Move the grating carriage by turning the allen wrench until the beam is centered on the desired grating. Use the white light stripe from the synchrotron, which is visible on the edge.
- ▶ **DISENGAGE THE WRENCH AND MOVE IT CLEAR OF THE LEAD-SCREW SOCKET USING THE LINEAR-MOTION COLLAR.**
- ▶ Tell the computer which grating is selected using the main user-control panel.
- ▶ If the laser status indicator on the main user-control panel indicates an error, home the monochromator by clicking the "home" button located just below the laser status indicator. Wait for the monochromator to finish homing (a few minutes).

Monochromator
Tank



Selecting photon polarization

The beamline has an aperture which can select the photon polarization to be either left or right circularly polarized or linearly polarized in the horizontal plane. The degree of circular polarization is continuously variable. Three standard polarizations are available from the main user-control panel, which are suitable for many applications.

- ▶ To select left or right circularly polarized light with a degree of polarization of 0.80, click on the corresponding button on the main user-control panel.
- ▶ To select linear polarization with degree of polarization 0.9, click the corresponding button on the main user-control panel.

Selecting the slit movement mode

Both slits are moveable and are controlled automatically by the beamline control system. The normal operating mode is "Exit Slit Only," which fixes the entrance slit at the vertical focus of the beam to allow maximum flux, and moves the exit slit to maintain the focal conditions of the spherical grating. This mode is suitable for most experiments and the resolving power settings for the slit openings are calibrated for this mode.

Two other slit-move modes are available. One is "Rowland Circle" mode. This mode can be used for the most demanding resolution requirements. It positions the exit and entrance slits such that additional aberrations in the SGM optical system are cancelled. There is a loss of flux due to the movement of the exit slit away from the vertical focus of the M2 mirror. The second mode is "No Slit Moves" mode. This mode may be useful if it is desired to scan the monochromator rapidly since there is no delay due to the motion of the slits. It is best to set the nominal energy in one of the other modes to position the slits, then change to the "No Slit Moves" mode for scanning.

- ▶ To select a slit movement mode, select the desired operation on the main user-control panel.

Opening the beamline to the ring and to the endstations

The beamline valves are all controlled by the PanelMate valve control panel. All valves are interlocked to prevent accidental venting of the beamline and to protect equipment from the white-light of the synchrotron beam.

Interlock faults indicate that a protection set-point has been exceeded and the affected valves will not open until the appropriate condition is restored and the alarm has been cleared on the PanelMate. Please contact the beamline scientist or control-room operator to reset any interlock faults which have occurred. While the PPS/ EPS logic does not allow anyone to erroneously or catastrophically reset or open a valve, any faults that occur should be brought to the attention of the beamline scientist.

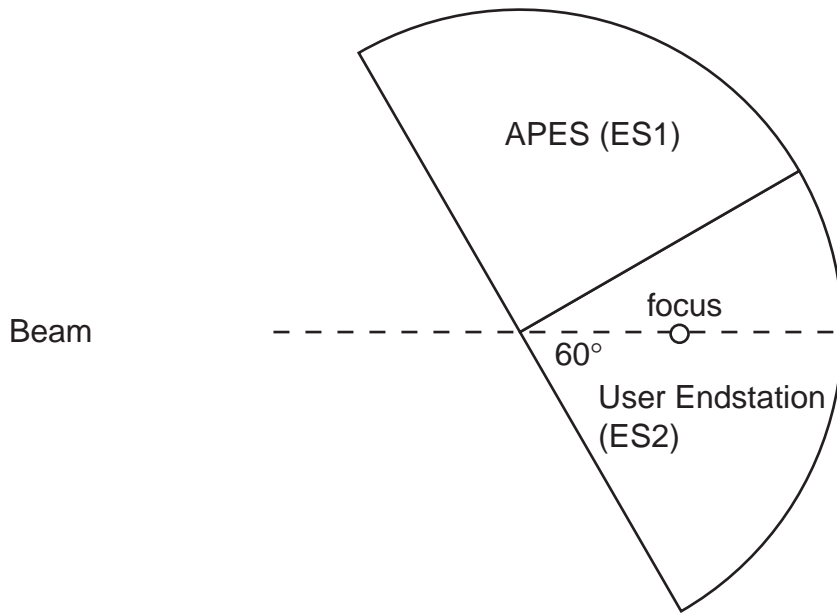


Beamline valve control panel and interlocked ion-gauges



Connecting a user endstation

A user endstation is placed on the endstation 2 (ES2) position of the platform. A 90 degree quadrant is available for the user chamber, minus a small portion of the center where the branch-line hardware is supported. An aluminum window valve is provided inline for vacuum separation if necessary. The branch line must remain at 10^{-9} Torr or less. Survey and alignment markers are available for precise chamber alignment. Contact the beamline coordinator or the survey and alignment team to make arrangements for online survey work.



- ▶ The connection to the beamline is a 2-3/4" conflat.
- ▶ The height of the conflat flange above the platform is 1.489 meters.
- ▶ The beam focus is 0.686 meters horizontally from the flange.
- ▶ The horizontal beam angle is 30° from the platform centerline.
- ▶ The beam focus is 1.434 meters vertically from the platform.
- ▶ The vertical beam angle is 4.6° down.
- ▶ The platform radius is 2.5 meters.
- ▶ The platform is 0.5 meters above the floor

Getting the beam into the endstation

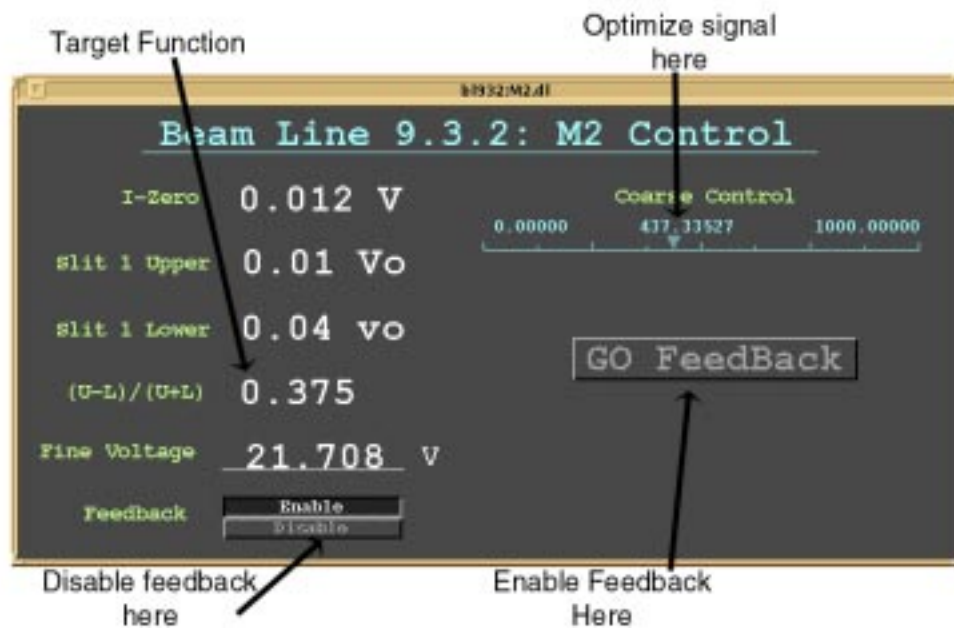
The endstations sit on a platform which can rotate without breaking the vacuum connections to the beamline. The endstations are numbered clockwise from the top starting with the position farthest from the ring. Currently, the APES endstation is endstation ES1, the AMC or user endstation position is ES2, and the FTSX interferometer is endstation ES3.

- ▶ Rotating the platform should be done with representatives of each of endstations ES1 and ES2 present.

Optimising the M2 feedback loop

The vertically deflecting mirror M2 has a piezo-electric drive which is used by the beamline control computer to maintain the beam on the entrance slit. Under normal operation this does not need to be adjusted by the user. The beamline scientist should optimise the feedback system once after each change in the operating mode of the synchrotron (electron energy, feed-forward on/off, etc.).

- ▶ Open the M2 feedback control window using the menu at the bottom of the main user control panel.
- ▶ Disable the feedback control by clicking the disable button.
- ▶ Adjust the mirror position using the slider control of the piezo voltage until the I-zero is maximised.
- ▶ If the “target function” is greater than 0.65 or less than -0.65, drag the slider back until the value is equal to the closest of these. This sometimes results in a loss of I-zero flux of ~10% but is necessary for stable operation of the feedback loop.
- ▶ Click the “Go Feedback” button.



Booting the beamline from scratch

The beamline may be brought into normal operation from any condition by following the procedure below.

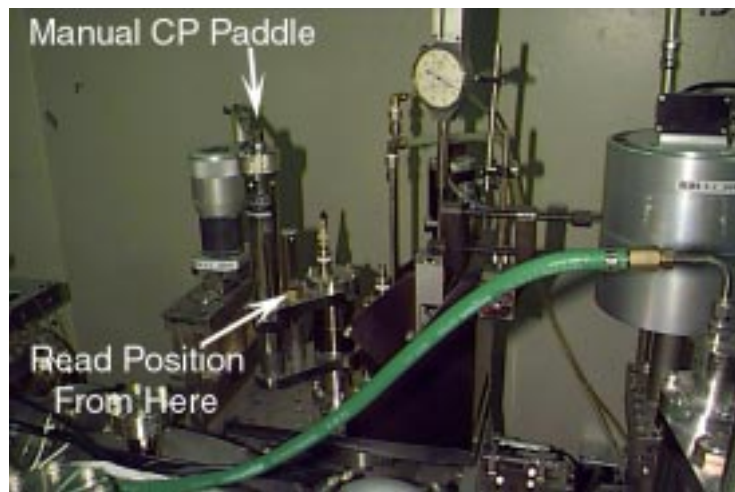
- ▶ Reboot the SUN workstation b193-102.als.lbl.gov.
- ▶ Logon to the user display-server and start the main user control panel.
- ▶ Reboot the VME crate by cycling the power. This takes about 5 minutes for all power-up procedures to be accomplished (homing motors, etc.).
- ▶ Open the valves from the ring up to the last endstation valve.
- ▶ Set the circular polarization to “Linear.” Note that you MUST click on the appropriate button even though it already displays the active selection as linear.



VME Crate

- ▶ Check that the manually moved circular-polarization paddle is set to 79 mm as read from the top of the bushing.
- ▶ Set the M1 mirror insertion(X) to -110,000. This control is available as a menu selection from the main user-control panel.

Circular Polarization Paddle



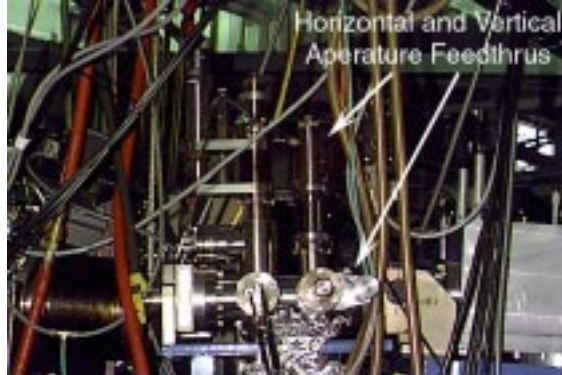
- ▶ Set the M1 mirror yaw to 10,000.
- ▶ Set the entrance slit opening to 16.25 mm.
- ▶ Select a grating.
- ▶ Set the photon energy to 65 eV for the 100 1/mm grating or 450 eV for the 600 1/mm grating.
- ▶ Set the exit slit opening to 15.5 mm.
- ▶ Set the Keithley current amplifiers which are reading the entrance slit currents to a gain of 10^4 V/A and filter constant of 100 msec.
- ▶ Check that the M4 deflection mirror for the FTSX endstation 3 is withdrawn.
- ▶ Optimise the M2 feedback by either optimising the I-zero signal or by getting the current from each slit approximately equal.
- ▶ Optimise the horizontal beam position by centering the beam on the paddle just upstream of the M3 refocussing mirror using the M1 Yaw adjustment. The paddle is inserted when reading 0.5" and is removed at 0.75".
- ▶ Check that the horizontal and vertical beam apertures in the I-zero section are withdrawn and clear of the beam.

M3 refocussing Mirror



- ▶ Optimise the M2 feedback by maximising the I-zero signal.
The beamline is now ready for operation.

I-Zero Section



Calibrating the Photon Energy

The photon energy calibration can shift whenever the grating is changed or when the synchrotron operating mode is changes. A routine is available for the 600 1/mm grating which will restore the energy calibration within ~25 meV. The routine is a labview VI which runs on the beamline SUN workstation. At a terminal prompt for a b1932usr login, type "cal600" without the quotation marks. The program can also be accessed from the PC at the beamline, just double-click the eXceed icon on the desktop labelled "b1932cal600.xs" This starts the labview program. The VI is located in the directory ~b1932usr/BL932/labview_stuff and is called SGMscans.vi. Directions for using the program are on the front panel.

Caveats and Known Problems

- ▶ The entrance Slit S1 is known to generate a motor fault occasionally after homing. Check the LN drive for a red fault light. The drive is located in the adjacent rack and is visible from the front. If the fault light is red, cycle the power to the drive and re-home the monochromator.
- ▶ Homing the monochromator will generate a calibration shift relative to its previous value. This is due to the finite accuracy of the homing switch.
- ▶ The monochromator calibration is fairly stable and reproducible, but there are changes that occur when the synchrotron changes energy and/or operating modes.
- ▶ Manuals cannot cover all possible situations or confer the benefit of all of the beamline scientists' experiences. If you are uncertain about or uncomfortable with any action with the beamline, please call the beamline scientist and ask, that is their job.

Other Technical Details

Directories and files of the user interface

The user interface is in the directory ~bl932usr/BL932/dl. The main window is in the file bl932.dl. All of the interface windows were created using EDD from the EPICS package.

VME crate and code

The crate is located in rack bl9035. It houses a Motorola MV167 CPU running VxWorks v5.1, a Xycom 566 A/D board, an HP10897A laser axis controller, and a D/A board. The crate boots up from machine bl93-102.als with the startup file in ~bl932usr/BL932/startup.cmd. Each sequencer program has an associated makefile with the name "Makesrcfilename".

Endstation Interface to monochromator control system

The monochromator control system can be accessed using either the simple channel access (SCA) utilities or by a serial connection. Contact an ALS controls group member for details regarding SCA. The serial connection is a 9600 8n1 port TTY1 connection to the back of the VME crate. The protocol uses C-strings. To request a monochromator energy setting, send the string "Exxx" where the "xxx" stands for any length decimal or integer number which is the photon energy desired in eV. For example, to request 400.5 eV, send "E400.5" with the appropriate termination character of return, null, or linefeed. There is no answer returned for this request. To find out when the monochromator is done moving, poll with the message "E!" and a single character string is returned containing either "0" meaning the monochromator is still moving or "1" meaning the monochromator is finished moving to the last requested energy. The current energy setting can be read by sending "E?" with the answering string being an ASCII representation of the decimal number, e.g. "400.49".

Optics

The information appearing on subsequent pages is an edited and updated version of LSBL-336.

Summary of Each Optical Element

The beamline operates under ultra-high vacuum and has a base pressure better than 60 nPa ($\sim 5 \times 10^{-10}$ Torr or $\sim 6 \times 10^{-10}$ mbar). For earthquake safety, the vacuum chambers are supported by the ALS orthogonal six-strut system designed to withstand 1 g of lateral acceleration (0.7 g is the ALS requirement). The stands for the mirrors and slits have a first vibrational mode higher than 30 Hz.

The grating tank stand legs are 30 cm outer diameter with a 2.5 cm wall thickness and are filled with water for thermal stability. The grating tank stand was only partially re-designed in moving to the ALS and the first mode of vibration is 23 Hz. All six struts supporting the grating tank, as well as the vertical struts of S1 and S2, are made of invar for stable energy calibration and reproducibility.

Fiducial points on each optical component are referenced to points on each respective vacuum tank for alignment. The ALS Surveyors aligned the optics to within 100 μm of the desired position based on ray tracing analyses of the beamline. Further alignment was completed by measuring the $\text{N}_2(\text{g})$ 1s to π^* resonance to monitor the resolution as well as scanning the intensity at various points along the beamline. (*Heimann 1990*)

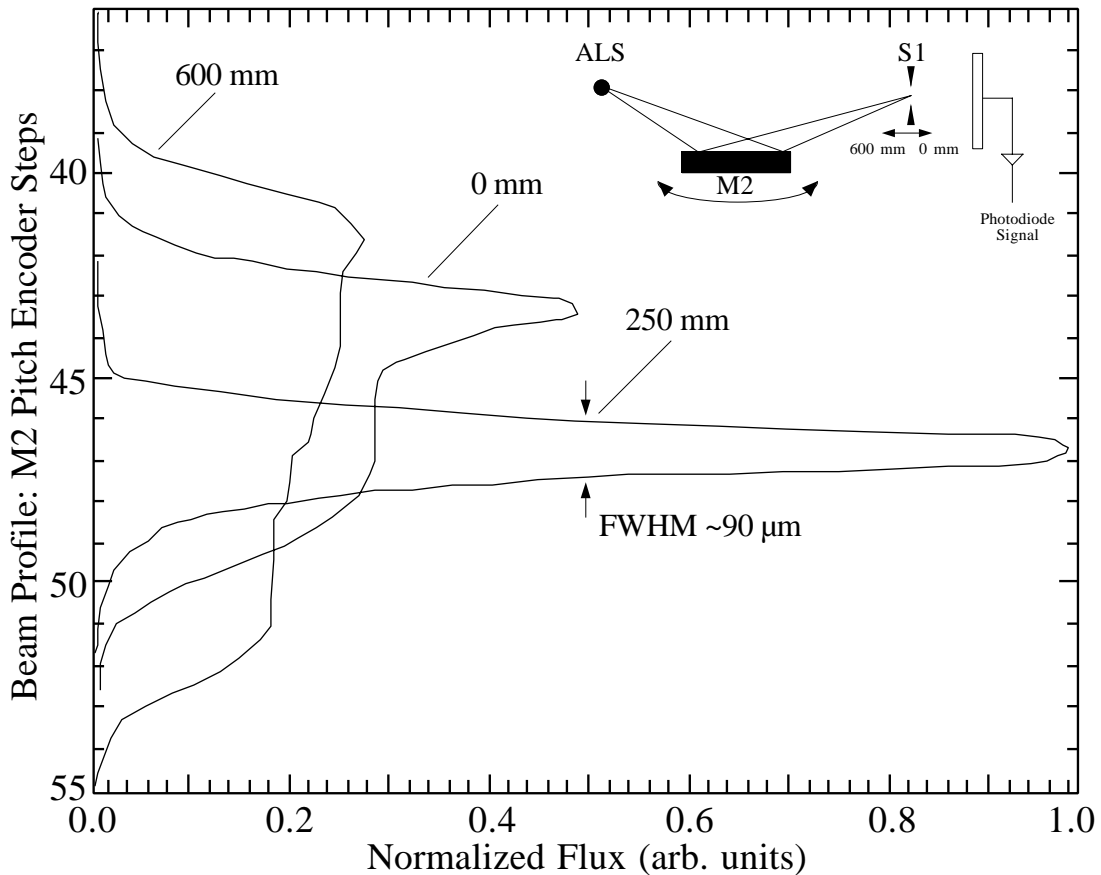
When discussing optic alignment and position, BL 9.3.2 conforms to the ALS standard notation regarding optical alignment. 'X' is horizontal motion perpendicular to the photon path. 'Pitch' is rotation about the X-axis. 'Y' is vertical motion. 'Yaw' is rotation about the Y-axis. 'Z' is motion along the photon path. 'Roll' is rotation about the Z-axis.

	MIRRORS			GRATINGS		
	M1	M2	M3	G100	G600	G1200
Shape	Tangenti al Cylinder	Sphere	Bent Cylinder	Sphere	Sphere	Sphere
Radius (m)	243 (design) 234 (actual)	243 (design) 242 (actual)	80 - ∞ (meridian) 0.1 (sagittal)	55	55	55
Incidence Angle	2.5°	2.5°	1° to 3°	Variable	Variable	Variable
Size (mm ³)	1200 × 100	400 × 75 × 70	400 × 40 × 7	188 × 100	188 × 100	188 × 100 × 50
Water Cooling	Yes	No	No	Yes	No	Yes
Bulk Material	Glidcop	Glidcop	ULE Quartz	Glidcop	ULE Quartz	Glidcop
Surface Material	250 Å Pt	250 Å Pt	250 Å Pt	250 Å Pt	250 Å Au	250 Å Pt
RMS Slope Error	<10 μrad	<0.6 μrad	≤5 μrad	≤1 μrad	≤1 μrad	≤1 μrad
RMS Roughness	5 Å	3 Å	5 Å	5 Å	5 Å	5 Å
Magnifi-cation	2.68	0.6	0.23 (meridian) 0.34 (sagittal)	---	---	---
Manufac-turer	Rockwell Internat'l	Rockwell Internat'l	Conti-nental Optics	Hyperfine	Ferranti Astron Ltd.	Hughes
Delivered Date	1993	1993	1996	1991	1988	1994

Kirkpatrick-Baez Deflection Mirrors

Because BL 9.3.2 is a bending magnet beamline, the source is a wide fan of radiation. M1 is a water-cooled tangential cylinder accepting 7.5 mrad of the horizontal radiation fan; this is determined by its length (1.2 m) and its location (7 m from the source) and the radiation incidence angle (2.5°). M1 focuses the beam horizontally near the exit slit (S2) with a magnification of 2.68. The M1 radius was designed to be 242 m; the delivered radius was 234 m. The focus was thus moved closer to the mirror by 2.8 m. The divergence angles are small which means M1 has a large depth of field. Subsequently, the effects of the slightly wrong radius are small. The present M1 has a fixed geometry. However, if one wished to optimize the radius, M1 and the front end could be designed such that it included an attached bender thus allowing the M1 radius to be adjusted. Such a bender is used during the polishing process. An alternative option is to employ a type of mirror recently designed by Malcolm Howells where the entire mirror is constructed as a flexure. (*Howells 1995*)

Completing the Kirkpatrick-Baez design is the spherical mirror M2 (242 m radius) which focuses the beam vertically at the midpoint of the entrance slit (S1) travel with a magnification of 0.60. M2 accepts 1.2 mrad of the vertical radiation fan ($2\theta = 5^\circ$). The vertical beam should be focused at S1 to obtain high throughput with a narrow slit width for maximum resolution. The M2 focal point was measured using a photodiode directly downstream of S1. With S1 at $10\ \mu\text{m}$, the M2 pitch was adjusted to scan the photon beam profile across the slit gap. The S1 position was changed after each scan and thus the focal point was experimentally determined to be 8.52 m downstream of M2 (0.07 m toward the grating tank from the design specification).



With S1 at $10 \mu\text{m}$, the M2 pitch was adjusted to scan the photon beam profile across the slit gap. The S1 position was changed after each scan and thus the focal point was experimentally determined to be 8.52 m from M2 (0.07 m toward the grating tank from the design specification). At the S1 travel extremes, the photon beam is out of focus shown by the broad, low intensity curves.

At the S1 travel extremes, the photon beam is out of focus shown by the broad, low intensity curves. The M2 radius is fixed; thus, the focal point is only very slightly adjustable by changing its elevation which changes the angle of incidence.

Gratings

Using one of three gratings, the accessible energy range is 30 eV to 1500 eV. The gratings are kinematically mounted onto a carriage attached to a rail by ball bearing rollers and their rotation is monitored with a laser interferometer. (McKinney 1990) The flux vs. energy for each grating is measured from a gold photodiode downstream from S2. (Krumrey 1992) Each spherical grating is designed to have a 55 m radius. The fixed included angle is 174° . The fact that the flux from the high energy grating does not drop off indicates a large scattered light component and a possible problem with the grating. A new grating has been ordered and should be installed in the Spring of 1999.

The grating alignment with respect to the photon beam has been described previously by McKinney *et al.* (McKinney 1990) After installation of the grating tank and prior to connecting the vacuum hardware from the slits, a HeNe laser beam was directed along the synchrotron beam path at the center of the grating. The roll and yaw of the gratings were

adjusted until the zeroth and ± 1 orders of diffraction fell on the same spot on a screen several meters away from the gratings. The 'Y' was adjusted so that this spot was stationary while changing the pitch, which is the motion used to scan the photon energy. It is extremely important that the gratings rotate about a grating line on the grating surface to maintain energy calibration and resolution.

SLITS

Each slit is based on a flexure design allowing a side-driven micrometer to push the jaws open vertically against spring tension continuously from $\leq 3 \mu\text{m}$ to $1500 \mu\text{m}$. The jaws are maintained parallel (within $\pm 1 \text{ mrad}$) over the full horizontal width of the beam, $\leq 10 \text{ mm}$. The jaws must also be parallel with the grating lines or else the slit width is effectively widened and the energy resolution is degraded.

The vertical struts on the entrance and exit slits are almost 1.3 m long on average. To maintain high stability in the energy calibration and energy resolution, the slits have to be vertically stable and thermal expansion of these struts was a concern. Thus, the vertical struts on the entrance and exit slits are constructed from invar so that the thermal expansion is negligible.

To satisfy the Rowland circle condition over a wide energy range, the entrance and exit slits are translatable over 600 mm and 1000 mm, respectively. BL 9.3.2 has three modes of operation: fixed slits, scanned slits (Rowland circle), and scanned exit slit (focus condition). The fixed slits mode is appropriate when a small energy range is being scanned. For best resolution, the slits should be set as close to the Rowland circle or the focus condition as possible. The full energy range of each grating can be reached under the focus condition by moving S1 away from the M2 focus and thus sacrificing some flux. The following table gives the energy range for each grating under the focus condition and the Rowland circle condition. These ranges are limited by the entrance slit's translation limits.

Energy Range of Beamline 9.3.2

Grating (lines/mm)	Focus Condition Energy Range (eV)	Rowland Circle Energy Range (eV)
100	30 - 150	45 - 77
600	200 - 800	270 - 460
1200	400 - 1500	540 - 920

It is critical that the slits' translation lie along the photon beam path. If S1 does not, then more or less of the beam centroid will be accepted which will adversely affect the flux. This is especially true for higher photon energies where the vertical divergence is less and effective size of the beam at S1 is smaller. If the S2 pitch is wrong, then the S2 position will be incorrect for a given photon energy. Additionally, if S1 and/or S2 do not travel along the beam path, then the energy calibration will change due to the changing included angle.

The Refocusing Mirror M3

The refocusing mirror is a bendable cylinder with a fixed small (sagittal) radius (10 cm) and an adjustable large (meridian) radius (80 m - ∞). The bending mechanism is based on a design by Howells (*Howells 1995*) and will allow for moving the meridian focus from 1.5 m to ∞ downstream of the refocusing mirror.

Foci Calculations

Horizontally Deflecting/Focusing Mirror, M1

The horizontally deflecting mirror, M1, is a tangential cylinder. It is curved in the horizontal plane which allows for horizontal focusing of the photon beam. This can be considered a two dimensional optical component and the meridian focal length, f_m , is defined by (*Michette 1986*)

$$f_m = \frac{R \sin \theta_i}{2} \quad (B1)$$

where R is the radius of curvature and θ_i is the angle of incidence as measured from the surface tangent at the mirror center. Using equation (B1) together with

$$\frac{1}{d_{\text{obj}}} + \frac{1}{d_{\text{img}}} = \frac{1}{f} \quad (B2)$$

where d_{obj} and d_{img} are the distances from the mirror center to the object and the image, respectively, the parameters for M1 can be calculated. It is important to note that these calculations are for the optical path. The vertical deflections of M2, the gratings, and M3 will cause the optical path length to differ slightly from the floor distance. Also, note that the calculations presented here are approximate in that they do not consider the effects of the other optical elements. The actual parameters were obtained from calculations using SHADOW which included all of the optical elements.

The distance from the source to the mirror, $d_{\text{obj-M1}}$, is 7.00 m. It was desirable to position the M1 focal point at the center of the exit slit travel. Given that $2\theta = 5^\circ$ for both M1 and M2, and the grating included angle is 174° (causing a net downward deflection of 1° from the grating center to the center of M3), the optical path length from the M1 center to the S2 travel center, $d_{\text{img-M1,design}}$, is 21.60 m. Using equation (B2), the desirable M1 meridian focal length is $f_{\text{m-M1,design}} = 5.29$ m. Rearranging equation (B1) and solving for the radius, $R_{\text{M1,design}} = 243$ m.

In fact, the actual M1 radius, $R_{\text{M1,actual}}$, is 234 m. The result of this -9 m deviation from the design value causes the actual meridian focal length, $f_{\text{m-M1,actual}}$, to be 5.10 m. Thus, the actual M1 focal point is $d_{\text{img-M1,actual}} = 18.79$ m, which is 2.8 m upstream of the S2 travel center.

The magnification, M , can be calculated by taking the ratio of the object and image distances.

$$M = \frac{d_{\text{img}}}{d_{\text{obj}}} \quad (\text{B3})$$

Thus, M1 magnifies the source by a factor of 2.68.

Vertically Deflecting/Focusing Mirror, M2

The vertically deflecting mirror, M2, is spherical and completes the Kirkpatrick-Baez design. (Michette 1986) It is curved in the vertical plane which allows for vertical focusing of the photon beam. As with M1, the meridian focal length, f_{m} , is defined by equation (B1).

It is desirable to vertically focus the photon beam at the center of the entrance slit travel to obtain high throughput with a narrow slit width for maximum resolution. Taking account of the 5° horizontal deflection of M1, the distance from the source to the M2 center, $d_{\text{obj-M2}}$, is 14.22 m. The distance from the M2 center to the S1 travel center, $d_{\text{img-M2,design}}$, is 8.45 m. Using equation (B2), the desired meridian focal length, $f_{\text{m-M2,design}}$, is thus 5.30 m. Using equation (B1), the desired radius, $R_{\text{M2,design}}$, is 243 m. It is purely coincidence that the M2 radius turns out to be the same as the M1 radius. The actual M2 radius is 242 m which causes the focal point to move closer to the mirror by a negligible 0.07 m.

In fact, the focal point of M2 is slightly adjustable by changing its elevation. Because M2 is spherical, $\theta_i = 2.5^\circ$ only at the mirror center. Lowering M2 causes θ_i to become larger (more incidence) which moves the focal point *away* from the mirror. Raising M2 causes θ_i to become smaller (more glancing) which moves the focal point *toward* the mirror. As described in the text, it was experimentally determined that $d_{\text{img-M2,actual}} = 8.52$ m downstream from M2. Using equation (B3), the magnification of M2 is 0.60 (the photon beam is $< \frac{2}{3}$ of the source size at the M2 focus).

The fact that M2 is three dimensional must be considered. That is, the spherical surface will also cause focusing in the horizontal plane which is described by the sagittal focal length, f_s , where (Michette 1986)

$$f_s = \frac{R}{2 \sin \theta_i} \quad (B4)$$

Given that $R_{M2,actual} = 242$ m and $\theta_i = 2.5^\circ$, $f_{s-M2} = 2774$ m. Using equation (B2), the sagittal focal point, $d_{s,img-M2}$, is -14.29 m (14.29 m upstream of M2). This results in some astigmatism at the entrance slit. (*Michette 1986*)

The astigmatism would not have been present if a tangential cylinder had been used for M2 instead of a sphere. However, manufacturing considerations made a spherical mirror the better choice. A spherical mirror can be polished to much higher quality than a tangential cylinder. The aberrations at the focal point are a minor consideration when compared with the higher optical quality of the spherical mirror.

Refocusing Mirror, M3

The refocusing mirror, M3, is used to focus the beam both vertically and horizontally to the same point. It is desirable to have this point the same for each endstation on the platform. This will minimize the switch-over time between experimental stations. As determined by the permanently mounted Advanced Photoelectron Spectrometer/Diffractometer, (*Ynzunza to be published*) the focal point should be 2.17 m downstream from the M3 center. At the largest angle of incidence, M3 deflects the beam vertically by -3° (in addition to the net -1° downstream of the grating). Since 4° is such a small angle, this floor distance and the optical path length are the same to the nearest 0.01 m.

To place both the meridian and sagittal focal points at the same place in space, the vertical and horizontal curvatures must be different. To accomplish this task with a single mirror, either a toroid or a bent cylinder must be used. Manufacturing costs and delivery times dictated the choice of using a bent cylinder. The large (meridian) radius is adjustable while the small (sagittal) radius is fixed.

Because M3 is a vertically deflecting mirror, equations (B1) and (B2) can be used to determine the desired long radius and thus the bending parameters. The focal distance, $d_{m,img-M3}$, is 2.17 m as stated. The object distance, $d_{m,obj-M3}$, is the distance from the M3 center to the travel center of S2 (the closest vertically defining aperture) which is 3.60 m. Thus, the meridian focal length of M3, f_{m-M3} , should be 1.35 m. With $\theta_i = 1.5^\circ$, the long (meridian) radius of M3, R_{m-M3} , should thus be bent to 103 m.

Similarly, equations (B4) and (B2) can be used to determine the desired short radius of M3. The focal distance $d_{s,img-M3}$, is also 2.17 m as stated. The object distance $d_{s,obj-M3}$, is the distance from the M3 center to the grating center, 7.80 m. Thus, the sagittal focal length of M3, f_{s-M3} , should be 1.70 m. With $\theta_i = 1.5^\circ$, the short (sagittal) radius of M3, R_{s-M3} , should thus be polished to 0.09 m.

The vertical and horizontal magnifications can be calculated using equation (B3) and the distances already mentioned. The vertical magnification, $M_{m-M3} = d_{m,img-M3}/d_{m,obj-M3}$, is 0.60 while the horizontal magnification, $M_{s-M3} = d_{s,img-M3}/d_{s,obj-M3}$, is 0.28. These multiply to the exit slit width and the horizontal size at the grating respectively.

Monochromator Calculations

Michette (Michette 1986) and Kunz *et al.* (Kunz 1979) are good references for a detailed discussion of the Rowland circle optical configuration, including image distortion and focusing. Here, the Rowland circle will be discussed with regard to BL 9.3.2.

Figure C1 illustrates how the Rowland circle applies to BL 9.3.2. The grating radius, R_G , is fixed at 55 m; thus, the Rowland circle radius, $R_G/2$, is fixed at 27.5 m.. For a spherical concave grating, the grating equation is the same as that for a plane grating (Kunz 1979)

$$\sin \alpha + \sin \beta = \frac{(\pm m)\lambda}{d} \quad (C1)$$

where α and β are the incident and reflected angles, respectively, as measured normal to the grating surface at its center, λ is the wavelength of the light, m is an integer specifying the diffraction order and is positive if $|\alpha| > |\beta|$, and d is the spacing between lines on the grating. For the 100 lines/mm grating, d is 1.00×10^5 Å; for the 600 lines/mm grating, d is 1.67×10^4 Å; for the 1200 lines/mm grating, d is 8.33×10^3 Å.

BL 9.3.2 is a fixed included-angle Rowland circle spherical grating monochromator (SGM). The condition holds that

$$\alpha - \beta = 2\theta \quad (C2)$$

where 2θ is the included angle ($2\theta = 174^\circ$ for BL 9.3.2). An alternative design, the variable included-angle SGM, does not conform to the Rowland circle geometry. (Petersen 1995) The included angle is determined by considering such things as the grating radius and the desired reflectivity, i.e., the highest desired photon energy for a given line spacing. Equation (C2) is written $\alpha - \beta$ because β is defined to be negative. This sign convention follows from the definitions of the outside order and the inside order. (Kunz 1979; Hogrefe 1986; Michette 1986)

By using the trigonometric identity

$$\sin \alpha + \sin \beta = 2 \sin \left[\frac{1}{2} (\alpha + \beta) \right] \cos (\alpha - \beta) \quad (C3)$$

equations (C1) and (C2) can be solved simultaneously and to determine α and β .

$$\alpha = \sin^{-1} \left[\frac{m\lambda}{2d \cos \theta} \right] + \theta \quad (C4a)$$

$$\beta = \sin^{-1} \left[\frac{m\lambda}{2d \cos \theta} \right] - \theta \quad (C4b)$$

For a known line density and a known inclusion angle, the slit positions can now be calculated for given photon energy. The focus condition for the Rowland circle mounted SGM in the dispersion plane is defined as

$$\frac{\cos^2 \alpha}{r_{S1}} - \frac{\cos \alpha}{R_G} + \frac{\cos^2 \beta}{r_{S2}} - \frac{\cos \beta}{R_G} = 0 \quad (C5)$$

where r_{S1} and r_{S2} are the distances from the grating center to S1 and S2 respectively. The Rowland circle condition is a special case of the focus condition where

$$r_{S1} = R_G \cos \alpha \quad (C6a)$$

$$r_{S2} = R_G \cos \beta \quad (C6b)$$

The effects of aberrations on the resolution, including the primary coma, the spherical aberration, the line curvature and the slit-width, can be calculated using the discussion by Hogrefe, *et al.* (Hogrefe 1986) along with a discussion by Howells in section 5 of the X-Ray Data Booklet. (Kirz 1986) The wavelength broadening due to the *primary coma* is described by

$$\Delta\lambda_{PC} = \frac{3w^2 d}{2m} \sum \left(\frac{T_{S1} \sin \alpha}{r_{S1}} \right) \quad (C7)$$

The wavelength broadening due to the *spherical aberration* is described by

$$\Delta\lambda_{SA} = \frac{w^3 d}{2m} \sum \left(\frac{4T_{S1} \sin^2 \alpha}{(r_{S1})^2} - \frac{(T_{S1})^2}{r_{S1}} + \frac{S_{S1}}{(R_G)^2} \right) \quad (C8)$$

Assuming a point source illumination, the wavelength broadening due to the *line curvature* is described by

$$\Delta\lambda_{LC} = \frac{\ell^2 d}{2m} \left[\sum \left(\frac{S_{S1} \sin \alpha}{r_{S1}} \right) - \frac{2 \sin \beta}{r_{S1}} \sum (S_{S1}) + \sin \beta (\sum (S_{S1}))^2 \right] \quad (C9)$$

When discussing the broadening due to the finite slit width, Hogrefe, *et al.* (Hogrefe 1986) consider the entrance slit. However, Reich, *et al.* suggest that the slit-width limited resolution is due to the exit slit for a toroidal grating. (Reich 1993) From experience, it is known that both slit-widths affect the resolution. By quadratically summing the contribution from each slit, the *slit-width* limited resolution is described by

$$\Delta\lambda_{SW} = \sqrt{\sum \left[\left(\frac{W_{S1} d \cos \alpha}{mr_{S1}} \right)^2 \right]} \quad (C10)$$

where W_{S1} is the width of the entrance slit. For these equations, the Σ indicates that a second term must be added to the first term such that $r_{S1} \Rightarrow r_{S2}$, $\alpha \Rightarrow \beta$, $T_{S1} \Rightarrow T_{S2}$, $S_{S1} \Rightarrow S_{S2}$, and $W_{S1} \Rightarrow W_{S2}$. The variables T and S are described by

$$T_{S1} = \frac{\cos^2 \alpha}{r_{S1}} - \frac{\cos \alpha}{R_G(w)} \quad (C11a)$$

$$S_{S1} = \frac{1}{r_{S1}} - \frac{\cos \alpha}{R_G(\ell)} \quad (C11b)$$

Note that a sphere is a special case of a toroid where $R_G(\ell) = R_G(w)$.

As discussed elsewhere, BL 9.3.2 operates in one of three modes: Fixed Slits, Fixed Entrance Slit, and Rowland Circle. Using equations (C7), (C8), (C9), and (C10), the theoretical resolution of the monochromator is plotted in the figures below. The resolving power is defined as

$$\text{Resolving Power} = \frac{\lambda}{\Delta\lambda} = \frac{E}{\Delta E} \quad (C12)$$

thus allowing for calculating in terms of wavelength and then converting to energy for a convenient plot. The conversion factor for converting eV to Å is 12398.54 eV·Å. Figures C3, C4, and C5 plot ΔE_{FWZH} (Full-Width Zero Height) vs. E for each aberration and the slit-width limit as well as the sum of all the effects for each grating. One can see in figures C3, C4, and C5 that the slit limited resolution can be approached only when the Rowland circle condition is satisfied. The entrance and exit slit widths were fixed at 10 μm for all calculations. Note that 'G' indicates the grating center.

Figure C2 plots the theoretical resolution for the 100 lines/mm grating. The calculation in C2a was completed with both slits fixed; S1 was fixed 1.95 m upstream from G and S2 was fixed 3.81 m downstream from G. These slit positions satisfy the Rowland circle condition for 70 eV as can be seen on the plot (the primary coma drops to zero). The calculation in C2b was completed in the Fixed Entrance Slit mode. S1 was fixed at the M2 focus, 1.68 m upstream from G. The exit slit was allowed to scan from 3.7 m to 4.7 m downstream from G to maintain the focus condition dictated by equation (C5). With the entrance slit fixed at 1.68 m upstream from G, the Rowland circle condition is satisfied at 54.4 eV. The calculation in C2c satisfies the Rowland circle condition by allowing both slits to move as dictated by equations (C6a) and (C6b). Although the total energy range calculated matched the range for figures C2a and C2b, the Rowland circle condition was only satisfied from 44.9 eV to 76.7 eV due to the limited travels of S1 and S2. The entrance slit was allowed to vary from 1.43 m to 2.03 m upstream of the grating; the exit slit travel limits were the same as figure C3b. Note that for figures C2b and C2c, when a slit position was calculated to be outside the allowed travel range, it was simply fixed at the extremum closest to the calculated value.

Figure C3 plots the theoretical resolution for the 600 lines/mm grating. The calculation in C3a was completed with both slits fixed; S1 was fixed 1.90 m upstream from G and S2 was fixed 3.85 m downstream from G. These slit positions satisfy the Rowland circle condition for 400 eV as can be seen on the plot (the primary coma drops to zero). The calculation in C3b was completed in the Fixed Entrance Slit mode. S1 was fixed at the M2 focus, 1.68 m upstream from G. The exit slit was allowed to scan from 3.7 m to 4.7 m downstream from G to maintain the focus condition dictated by equation (C5). With the entrance slit fixed at 1.68 m upstream from G, the Rowland circle condition is satisfied at 326 eV. The calculation in C3c satisfies the Rowland circle condition by allowing both slits to move as

dictated by equations (C6a) and (C6b). Although the total energy range calculated matched the range for figures C3a and C3b, the Rowland circle condition was only satisfied from 269.7 eV to 460.3 eV due to the limited travels of S1 and S2. The entrance slit was allowed to vary from 1.43 m to 2.03 m upstream of the grating; the exit slit travel limits were the same as figure C3b. Note that for figures C3b and C3c, when a slit position was calculated to be outside the allowed travel range, it was simply fixed at the extremum closest to the calculated value.

Figure C4 plots the theoretical resolution for the 1200 $\frac{\text{lines}}{\text{mm}}$ grating. The calculation in C4a was completed with both slits fixed; S1 was fixed 1.90 m upstream from G and S2 was fixed 3.85 m downstream from G. These slit positions satisfy the Rowland circle condition for 800 eV as can be seen on the plot (the primary coma drops to zero). The calculation in C4b was completed in the Fixed Entrance Slit mode. S1 was fixed at the M2 focus, 1.68 m upstream from G. The exit slit was allowed to scan from 3.7 m to 4.7 m downstream from G to maintain the focus condition dictated by equation (C5). With the entrance slit fixed at 1.68 m upstream from G, the Rowland circle condition is satisfied at 652 eV. The calculation in C4c satisfies the Rowland circle condition by allowing both slits to move as dictated by equations (C6a) and (C6b). Although the total energy range calculated matched the range for figures C4a and C4b, the Rowland circle condition was only satisfied from 539.4 eV to 920.5 eV due to the limited travels of S1 and S2. The entrance slit was allowed to vary from 1.43 m to 2.03 m upstream of the grating; the exit slit travel limits were the same as figure C4b. Note that for figures C4b and C4c, when a slit position was calculated to be outside the allowed travel range, it was simply fixed at the extremum closest to the calculated value.

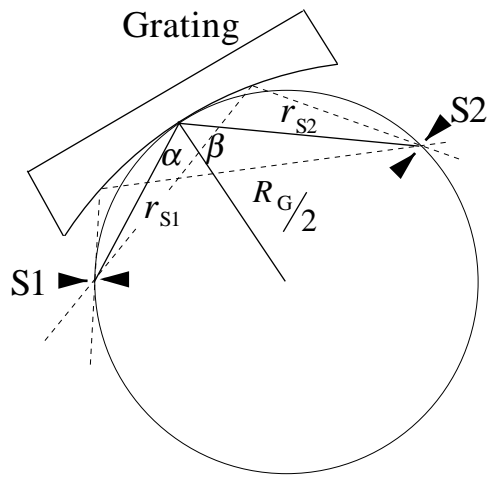
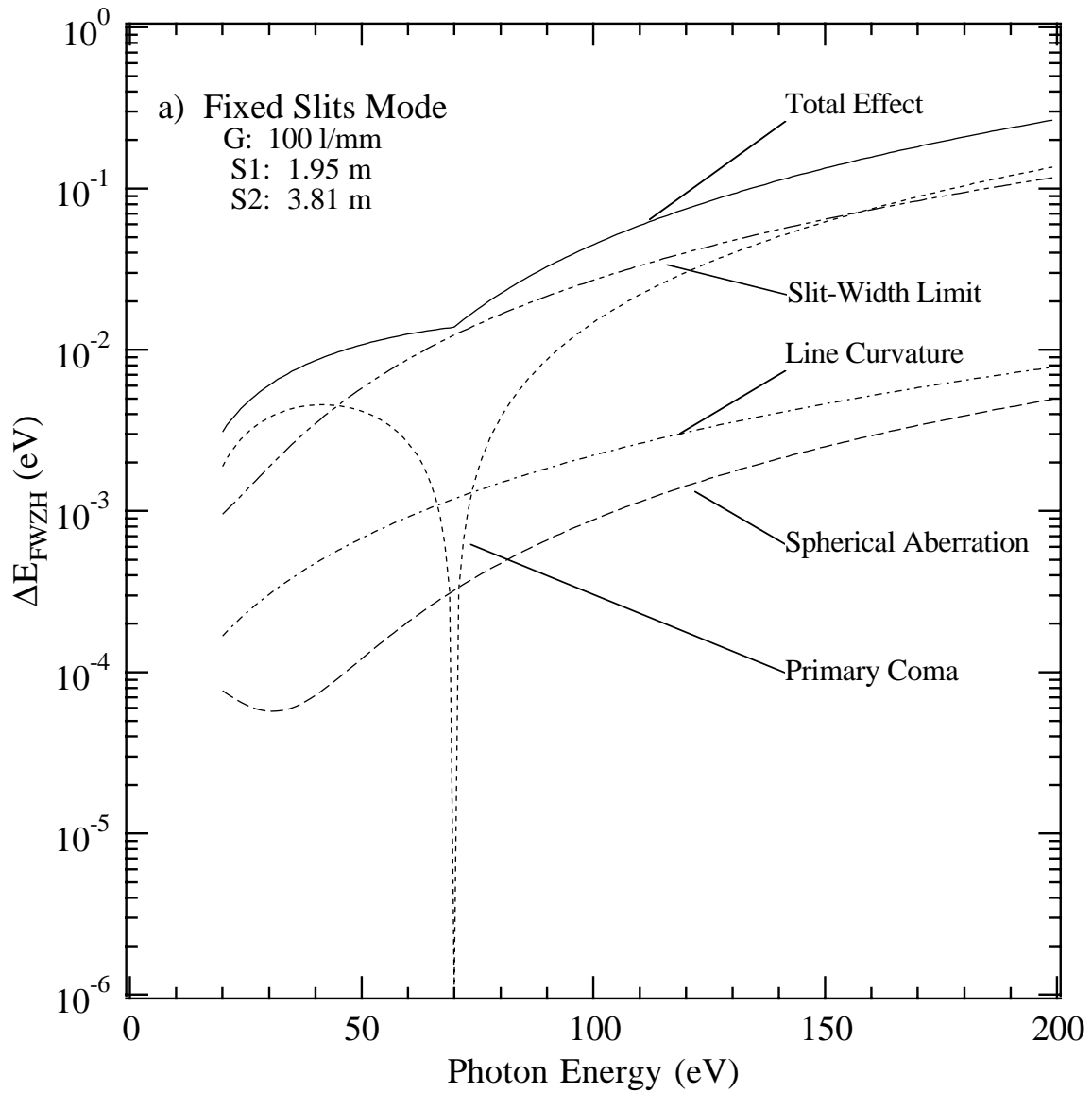
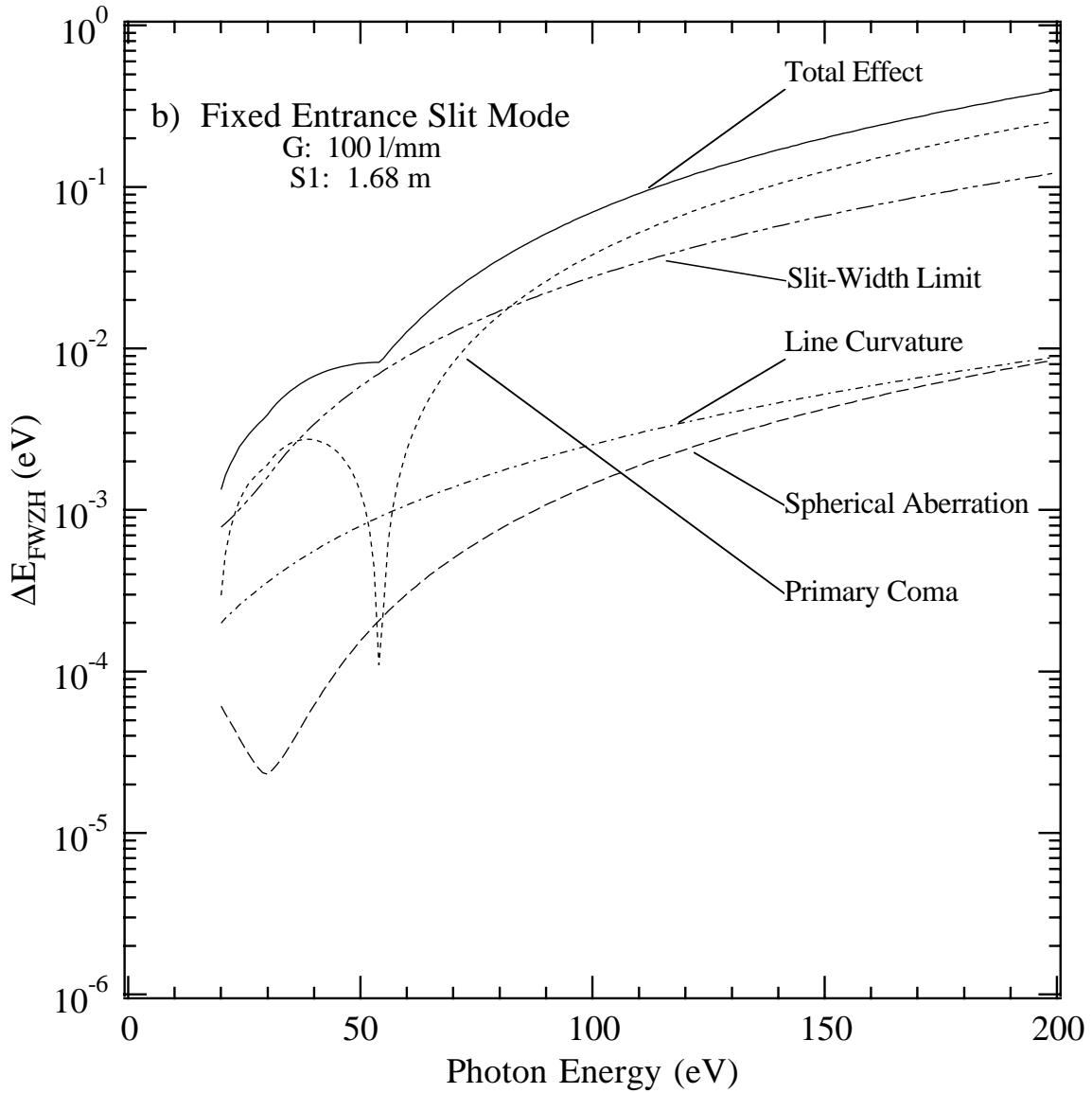


Figure C1



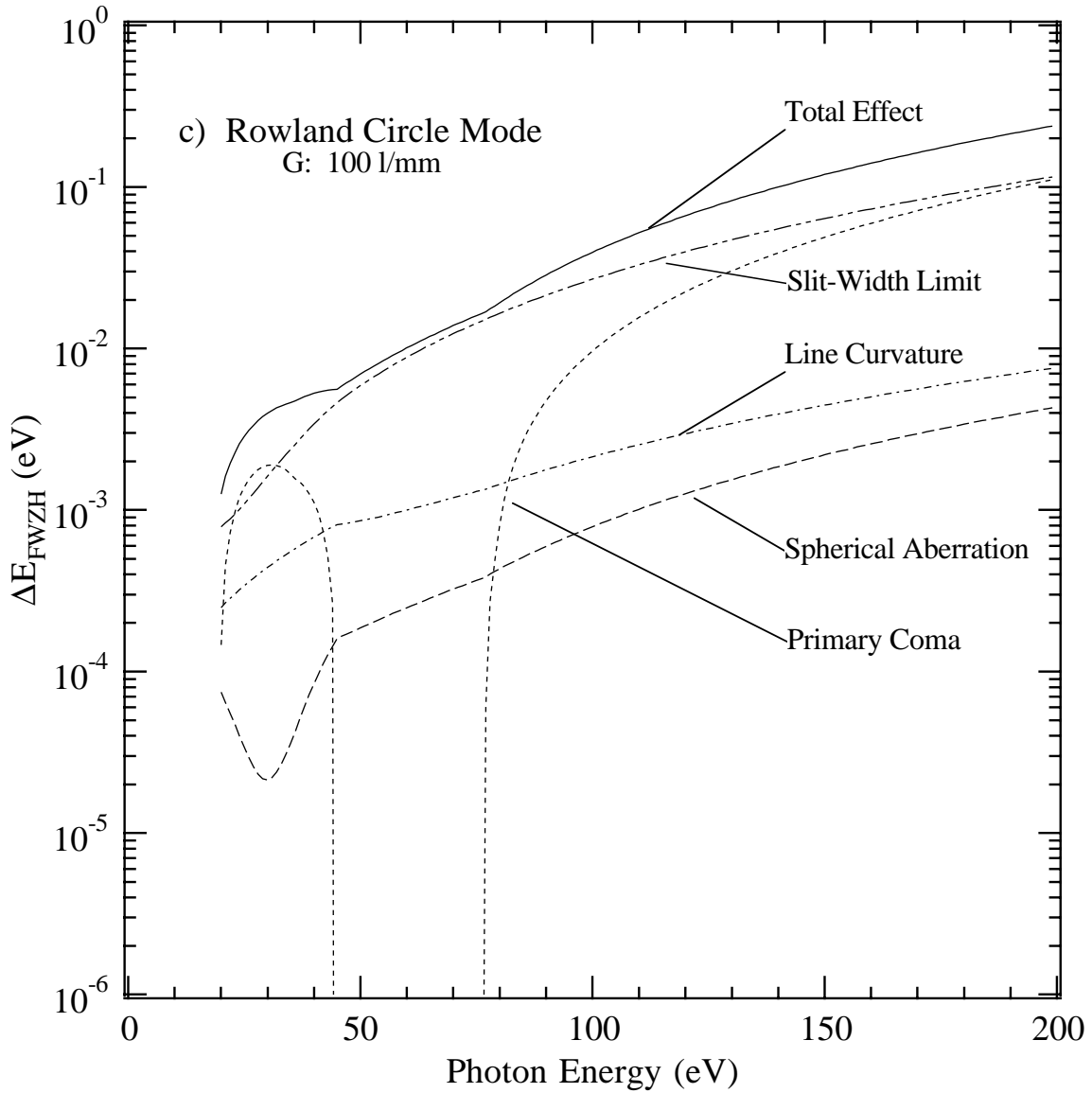
Calculation in Fixed Slits mode for the 100 $\frac{\text{lines}}{\text{mm}}$ grating. S1 was fixed at 1.95 m upstream from G and S2 was fixed at 3.81 m downstream from G. These positions satisfy the Rowland circle condition at 54.4 eV as evidenced by the primary coma dropping to zero at this energy. The entrance and exit slit widths were set to 10 μm .

Figure C2a



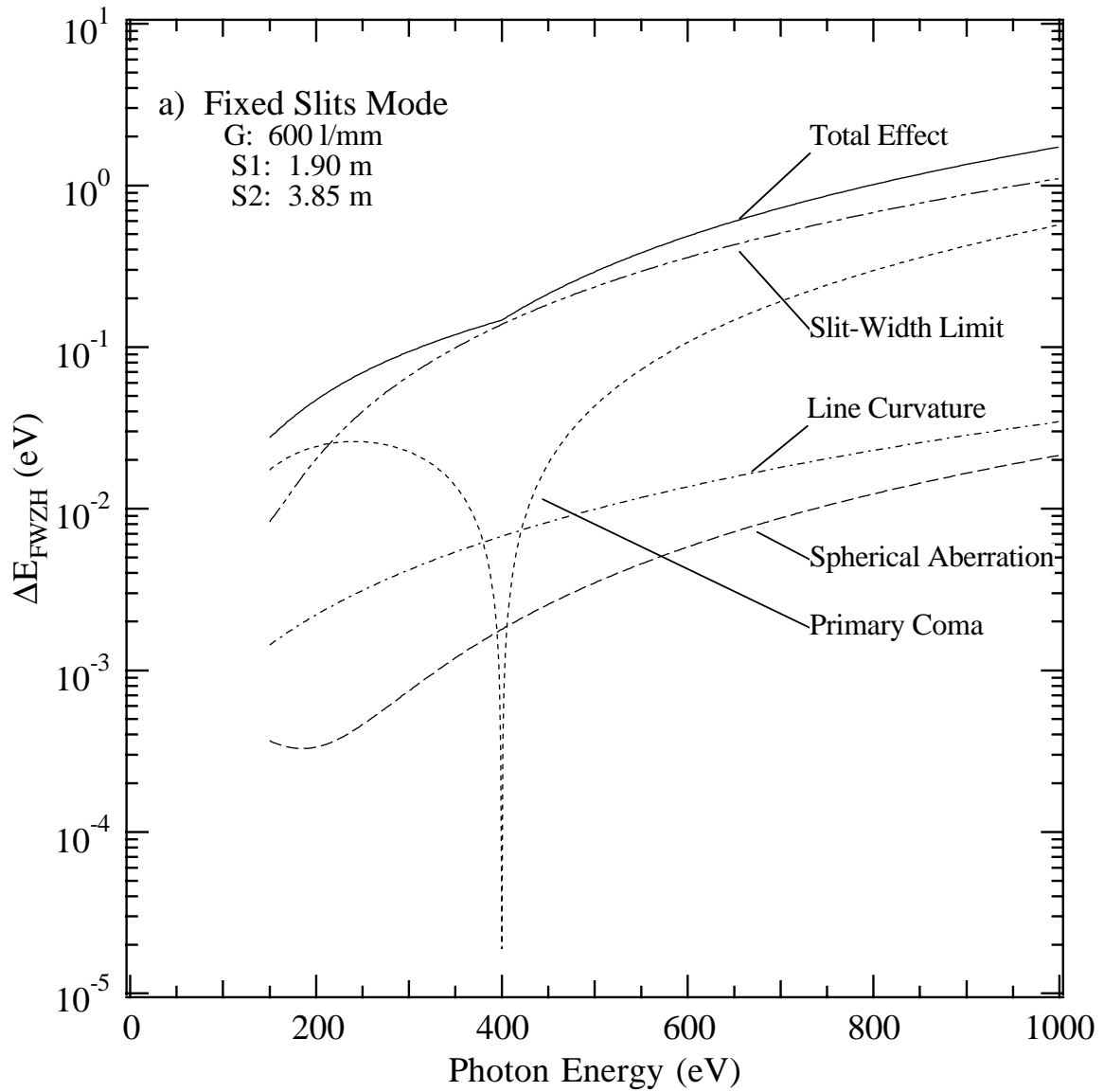
Calculation in Fixed Entrance Slit mode for the 100 $\frac{\text{lines}}{\text{mm}}$ grating. S1 was fixed at the M2 focus, 1.68 m upstream from G, and S2 was allowed to vary from 3.7 m to 4.7 m downstream from G. With S1 at 1.68 m, the Rowland circle condition is satisfied at 400 eV as evidenced by the primary coma dropping to zero at this energy. If the S2 position was calculated to be outside the allowed travel range, it was fixed at the extremum closest to the calculated value. The entrance and exit slit widths were set to 10 μm .

Figure C2b



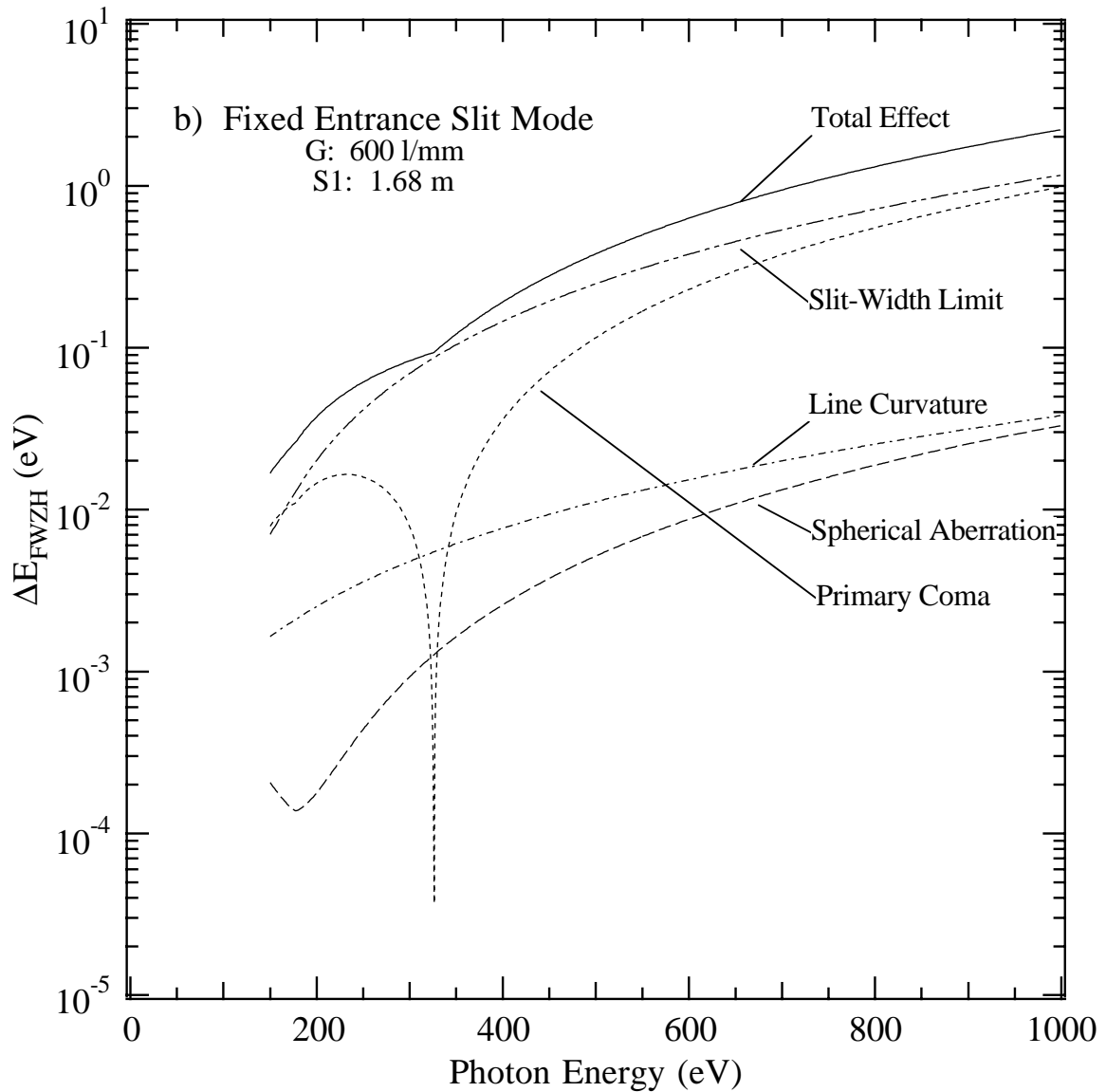
Calculation in Rowland Circle mode for the 100 $\frac{\text{lines}}{\text{mm}}$ grating. S1 was allowed to vary 1.43 m to 2.03 m upstream from G and S2 was allowed to vary 3.7 m to 4.7 m downstream from G. Although the energy range calculated matched that for figures C2a and C2b, the Rowland circle condition was only satisfied from 44.9 eV to 76.7 eV as evidenced by the primary coma dropping to zero in this range. If the S1 or the S2 position was calculated to be outside the allowed travel range, it was fixed at the extremum closest to the calculated value. The S1 and S2 slit widths were set to 10 μm .

Figure C2c



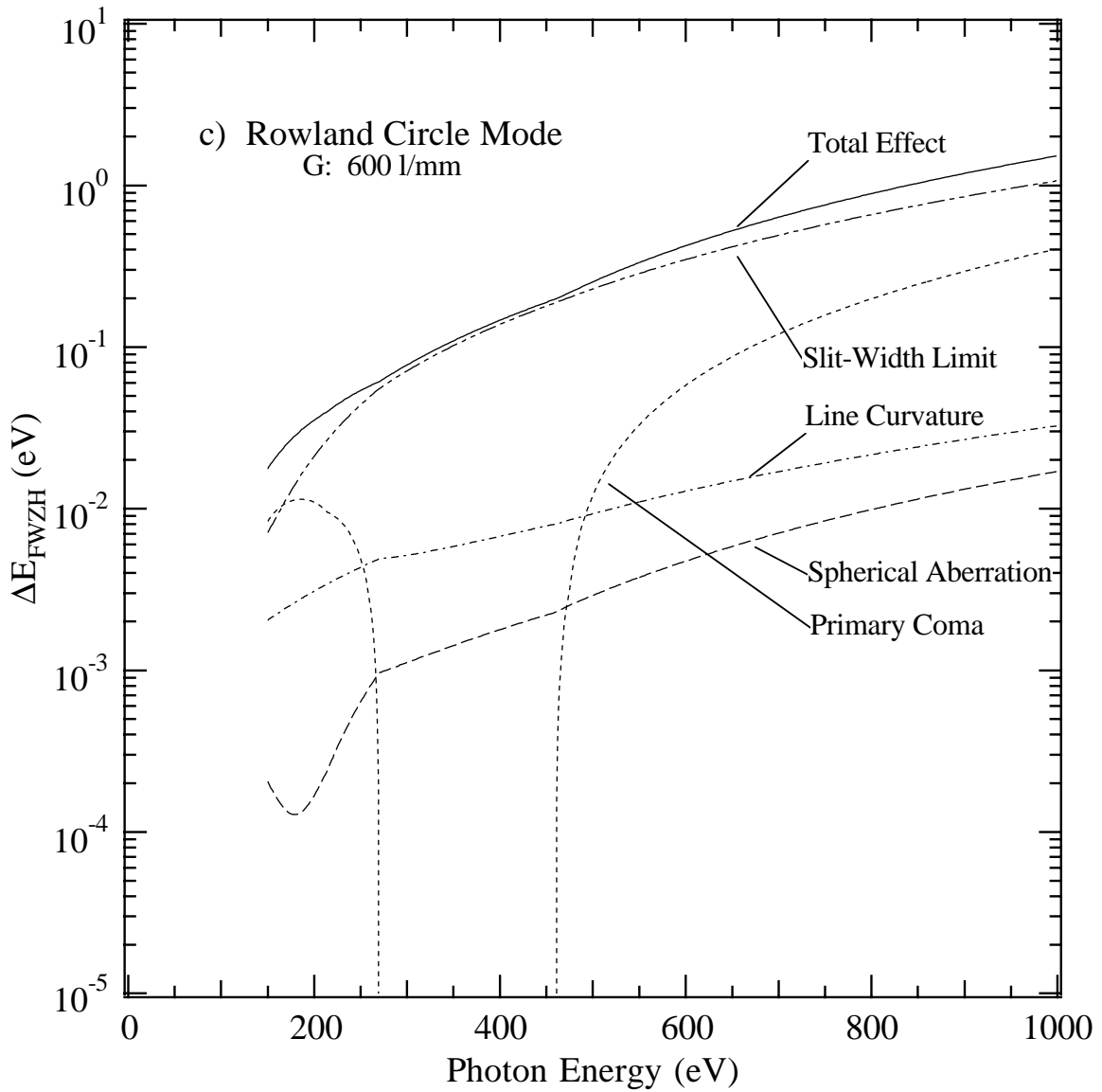
Calculation in Fixed Slits mode for the 600 $\frac{\text{lines}}{\text{mm}}$ grating. S1 was fixed at 1.90 m upstream from G and S2 was fixed at 3.85 m downstream from G. These positions satisfy the Rowland circle condition at 400 eV as evidenced by the primary coma dropping to zero at this energy. The entrance and exit slit widths were set to 10 μm .

Figure C3a



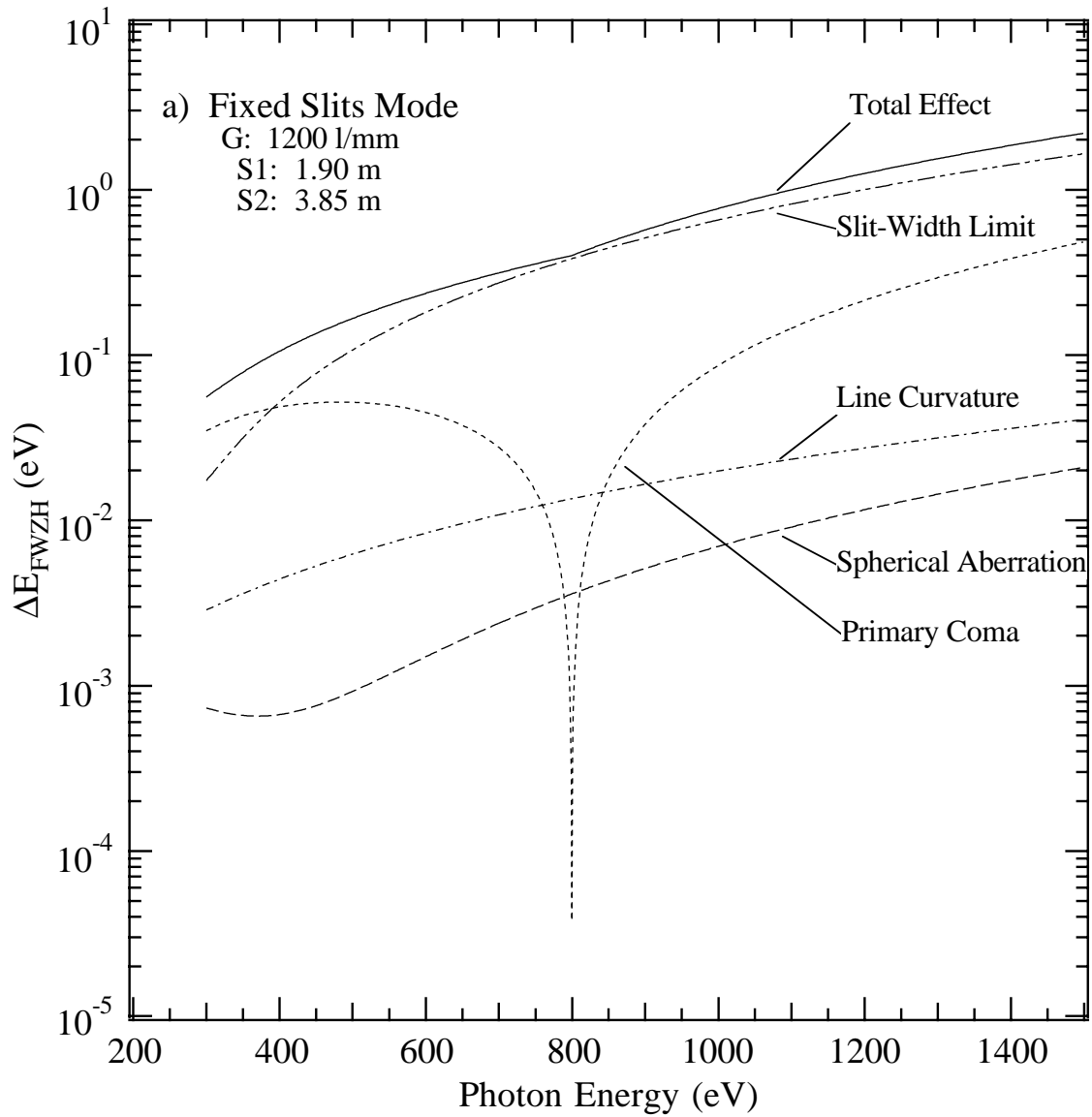
Calculation in Fixed Entrance Slit mode for the 600 $\frac{\text{lines}}{\text{mm}}$ grating. S1 was fixed at the M2 focus, 1.68 m upstream from G, and S2 was allowed to vary from 3.7 m to 4.7 m downstream from G. With S1 at 1.68 m, the Rowland circle condition is satisfied at 326 eV as evidenced by the primary coma dropping to zero at this energy. If the S2 position was calculated to be outside the allowed travel range, it was fixed at the extremum closest to the calculated value. The entrance and exit slit widths were set to 10 μm .

Figure C3b



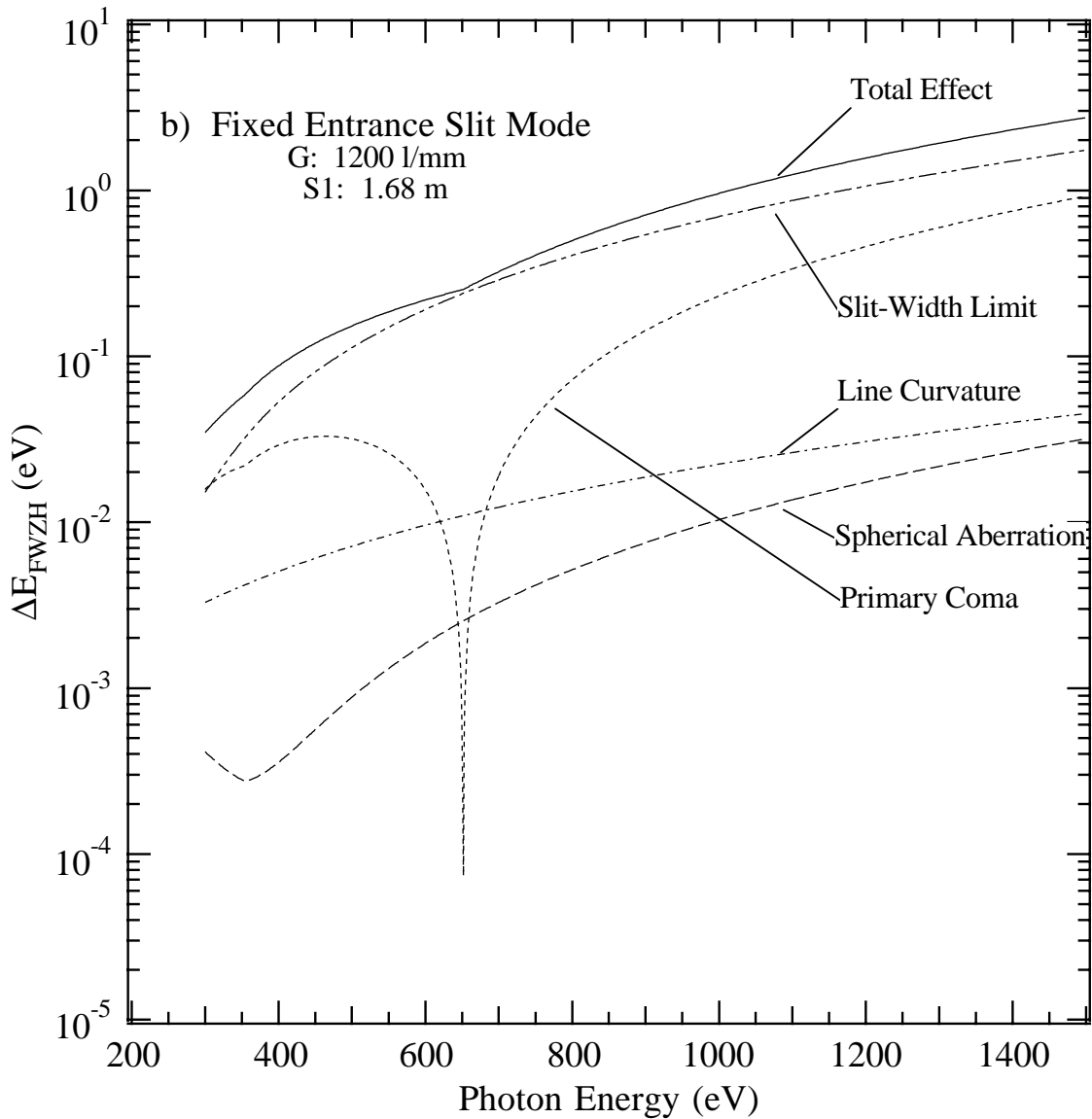
Calculation in Rowland Circle mode for the 600 $\frac{\text{lines}}{\text{mm}}$ grating. S1 was allowed to vary 1.43 m to 2.03 m upstream from G and S2 was allowed to vary 3.7 m to 4.7 m downstream from G. Although the energy range calculated matched that for figures C3a and C3b, the Rowland circle condition was only satisfied from 269.7 eV to 460.3 eV as evidenced by the primary coma dropping to zero in this range. If the S1 or the S2 position was calculated to be outside the allowed travel range, it was fixed at the extremum closest to the calculated value. The S1 and S2 slit widths were set to 10 μm .

Figure C3c



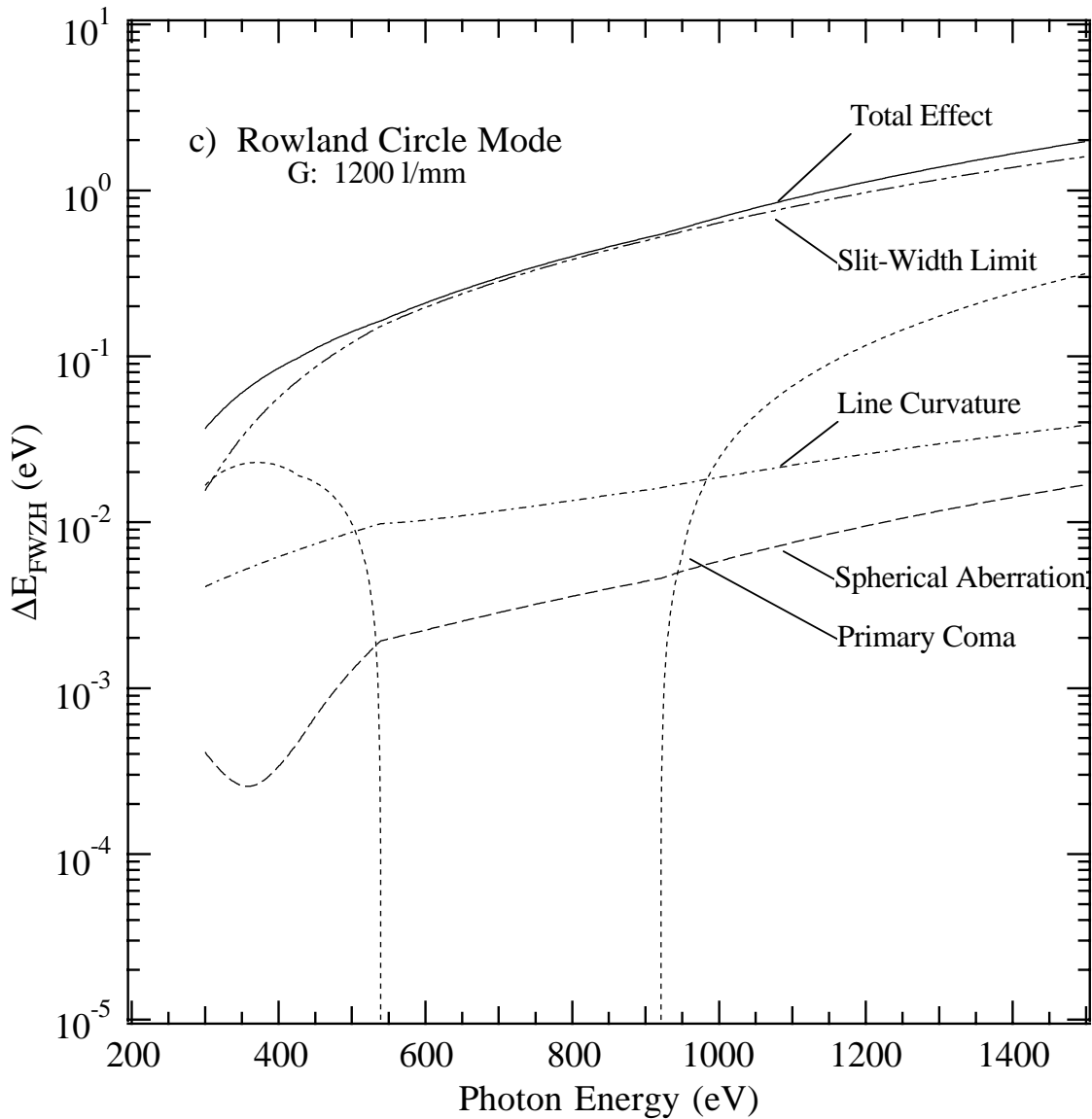
Calculation in Fixed Slits mode for the 1200 lines/mm grating. S1 was fixed at 1.90 m upstream from G and S2 was fixed at 3.85 m downstream from G. These positions satisfy the Rowland circle condition at 800 eV as evidenced by the primary coma dropping to zero at this energy. The entrance and exit slit widths were set to 10 μm .

Figure C4a



Calculation in Fixed Entrance Slit mode for the 1200 $\frac{\text{lines}}{\text{mm}}$ grating. S1 was fixed at the M2 focus, 1.68 m upstream from G, and S2 was allowed to vary from 3.7 m to 4.7 m downstream from G. With S1 at 1.68 m, the Rowland circle condition is satisfied at 652 eV as evidenced by the primary coma dropping to zero at this energy. If the S2 position was calculated to be outside the allowed travel range, it was fixed at the extremum closest to the calculated value. The entrance and exit slit widths were set to 10 μm .

Figure C4b



Calculation in Rowland Circle mode for the 1200 $\frac{\text{lines}}{\text{mm}}$ grating. S1 was allowed to vary 1.43 m to 2.03 m upstream from G and S2 was allowed to vary 3.7 m to 4.7 m downstream from G. Although the energy range calculated matched that for figures C4a and C4b, the Rowland circle condition was only satisfied from 539.4 eV to 920.5 eV as evidenced by the primary coma dropping to zero in this range. If the S1 or the S2 position was calculated to be outside the allowed travel range, it was fixed at the extremum closest to the calculated value. The S1 and S2 slit widths were set to 10 μm .

Figure C4c

Circular Polarization Calculations and Measurements

Calculations

Calculations were performed to determine how the flux and the degree of circular polarization vary as a function of photon energy for different beam-stop sizes introduced in the orbit plane. This beam-stop is used to exclude the horizontal polarization component. (Padmore 1993) As discussed in the text, different beam-stop sizes are introduced by a water-cooled, movable aperture which defines the lower (or upper) acceptance angle. The parallel polarized component (s) is at a maximum in the orbit plane and the perpendicular polarized component (p) is zero in the orbit plane but maximum at a small angle out of the plane. The value of the small angle where this maximum occurs is dependent on the photon energy. The beamline accepts radiation in the vertical direction from a lower angle, Ψ_l , defined by the position of the movable aperture to an upper angle, Ψ_u , defined by a mirror, a grating, or perhaps a real aperture. The flux through the aperture, F_a , is defined by

$$F_a = \int_{\Psi_l}^{\Psi_u} \frac{dF}{d\psi} d\psi \quad (D1)$$

where $\frac{dF}{d\psi}$ is the flux per unit vertical aperture as a function of the out of plane angle ψ and depends on the machine energy, the photon energy, the critical photon energy, the bending field strength, as well as the s and p polarized light components. (Green 1977)

$$\frac{dF}{d\psi} = 1.327 \times 10^{13} \left[\frac{VE}{E_c} \right]^2 \times [1 + X^2] \times [A_h^2 + A_v^2] \quad (D2)$$

where V (GeV) is the machine energy, E (eV) is the photon energy, and E_c (eV) is the critical photon energy. For a bending magnet, $E_c = 655V^2 B$ where $B(V, \rho)$ (T) is the bending magnet field strength and ρ (m) is the bend radius, 4.8 m for the *non*-superconducting magnets at the ALS. $X = \gamma\psi$ where $\gamma \equiv \frac{V}{m_e c^2}$, m_e is the electron mass ($5.11 \times 10^{-4} \text{ GeV}/c^2$) and c is the velocity of light. A_h and A_v represent the s and p polarized light components, respectively, such that

$$A_h = K_{2/3}(\xi) \quad (D3a)$$

$$A_v = \frac{X}{\sqrt{1 + X^2}} K_{1/3}(\xi) \quad (D3b)$$

where

$$\xi = \frac{E}{2E_c} (1 + X^2)^{3/2} \quad (D4)$$

and the K 's are modified Bessel functions of the second kind.

Considering only half-apertures above (or below--the argument is the same with simply the 'upper' and 'lower' reversed) the plane of the ring, ψ_ℓ is defined by the position of the aperture. The aperture is 13.4 m downstream from the source and is indicated on figure 1 of the main text. ψ_u is defined by the acceptance of M2, ϕ_{M2} , which is constant (0.6 mrad) or the acceptance of the grating, ϕ_G , which is a function of the photon energy, the grating width, and the beamline geometry. Accounting for the magnification of M2 (discussed in Appendix B),

$$\phi_G = \frac{w}{r_{S1,G}} \cos\left(\alpha \frac{r_{M2,S1}}{r_{S,M2}}\right) \quad (D5)$$

where w is the illuminated width of the grating and α is the angle of incidence on the grating (see Appendix C for a discussion). $r_{S,M2}$ is the source to M2 distance, $r_{M2,S1}$ is the M2 to entrance slit distance, and $r_{S1,G}$ is the entrance slit to grating distance. Although one may think in terms of 'length' being the longitudinal size of the grating, w (indicative of the number of illuminated grooves) was chosen to be consistent with the resolution calculations discussed in Appendix C and references therein. Thus, ψ_u is defined by the lesser of the two values ϕ_{M2} and ϕ_G . It should be noted that for the polarization measurements discussed below, M3 was a defining aperture at lower photon energies because its longitudinal length was so short. For the calculations compared with these measurements, an effective $\phi_{M2\text{-eff}} = 0.5$ mrad was used. M3 has since been replaced with a larger mirror and is no longer an aperture.

Figure D1 graphs the total calculated flux from equation (D1) considering a grating line density of 600 lines/mm, a fixed included angle of 174°, and operated in the $m = +1$ diffraction order. Figure D2 plots the calculated fraction of the total emitted flux accepted by the aperture. The half-apertures of the central stop are shown ranging from 0.0 to 0.5 mrad. Larger central stop sizes cause a significant flux reduction, especially at high energies.

The degree of circular polarization, P_C , where

$$P_C = \sqrt{1 - \left(\frac{F_s - F_p}{F_s + F_p}\right)^2} \quad (D6)$$

and F_s and F_p are the s and p polarized fluxes, respectively, was calculated as a weighted average of the circular polarization over the aperture. The weighting is due to the change in intensity of the s and p polarized components across the aperture. Thus,

$$\langle P_C \rangle_a = \frac{1}{F_a} \int_{\psi_l}^{\psi_u} P_c(\psi) \frac{dF}{d\psi} d\psi \quad (D7)$$

Figure D3 plots the calculated average degree of circular polarization for the aperture. For the largest stop size, the degree of circular polarization is greater than 0.9. Even with no stop, it is typically greater than 0.6 throughout the energy range.

To optimize the balance between the flux and the circular polarization, it is useful to calculate the merit function as described by

$$M = \langle P_C \rangle_a \sqrt{F_a/F_t} \quad (\text{D8})$$

where F_t is the total flux radiated by the source at the defined photon energy (see figure D4). The half-apertures of the central stop are shown ranging from 0.0 to 0.5 mrad. The merit functions over the half-aperture sizes 0.0, 0.1, and 0.2 mrad are within 10% of each other over the entire energy range. This insensitivity is caused by the balance of decreasing flux and increasing degree of circular polarization.

Measurements

Polarization and intensity measurements as a function of the vertical aperture were made using a recently developed multilayer polarimeter. (Kortright 1995; Kortright 1996) The polarimeter can utilize both a transmission multilayer phase retarder and a reflection polarizer or analyzer. Some recent polarimetry measurements using multilayers have used a retarder to help distinguish between possible unpolarized and circularly polarized radiation. (Kimura 1992; Fonzo 1994) A retarder was not used for the measurements presented here; the degree of unpolarized radiation was found to be immeasurably small. The retarder also enables the distinction between left and right circularly polarized radiation, which is not problematic for bend-magnet radiation.

Three multilayers with constant period were mounted on the polarizer stage. These were translatable to illuminate the different optics allowing polarimetry measurements at 367 eV and 722 eV without breaking vacuum. The beamline was tuned to these photon energies using the 600 lines/mm grating; the storage ring was operating at 1.9 GeV. The polarimeter was mounted in tandem with the APESD chamber. Fine adjustment of the polarimeter was accomplished with its own translation and tilt stages. Because the polarimeter was not at the M3 focus, the vertical position of its 2 mm entrance pinhole was re-optimized as the upstream vertical aperture position was changed to maximize flux through the pinhole.

Standard rotating analyzer ellipsometry techniques and expressions were used to collect and analyze the data. (Collett 1993) The data collected were the intensity entering the polarimeter (measured as a mesh current) and analyzer scans which record the intensity reflected from the polarizer as it rotates azimuthally about the beam direction. The reflected intensity normalized by the incident intensity as a function of azimuthal angle, α , is given by

$$I(\alpha) = S_0 \frac{R_s + R_p}{2} + [S_1 \cos(2\alpha) + S_2 \sin(2\alpha)] \frac{R_s - R_p}{2} \quad (\text{D9})$$

where R_s and R_p are the reflectivities of the s and p polarized radiation component from the polarizer. S_0 , S_1 , and S_2 are the first three of four Stokes parameters which

define the intensity and polarization state of the beam. Thus, the degree of linear polarization, P_L , was measured directly.

$$P_L = \frac{(S_1^2 + S_2^2)^{1/2}}{S_0} \quad (\text{D10})$$

For all measurements reported here, the linear component at $\pm 45^\circ$, S_2 , is negligible compared to the linear component at 0° and 90° , S_1 .

Circular polarization is represented by the fourth Stokes parameter, S_3 . The degree of circular polarization, P_C , is

$$P_C = \frac{S_3}{S_0} \quad (\text{D11})$$

P_C is determined from

$$P_L^2 + P_C^2 + (\text{amount of unpolarized radiation}) = 1 \quad (\text{D12})$$

but the amount of unpolarized radiation was negligibly small. Since P_L and P_C add in quadrature, they can be regarded as representing the amplitudes of the different polarization types and it is correct to refer to them as the *degree* of polarization and not the *percent* of polarization.

Polarimetry data taken as the narrow horizontal slit is stepped vertically across the beam are useful to determine the orbit plane, to set an upper limit on the amount of unpolarized radiation, and to measure the variation of polarization state with aperture position. Since the radiation is most linearly polarized in the plane of the electron orbit, measuring P_L as the narrow slit is scanned unambiguously determines the orbit plane. Using the maximum in an intensity measurement to determine the orbit plane can be misleading if the measurement is made downstream of optics that are poorly aligned with respect to the beam. Careful vertical alignment of each optical element in succession (using intensity signals) was conducted prior to polarimetry measurements presented below. After alignment, both intensity and polarization signals indicated that the optics were reasonably well centered on the beam.

Experimental and theoretical values for P_L and P_C vs. ψ at 367 eV and 722 eV are shown in figures D5a and D5b, respectively. In comparing theory with experiment, it was assumed that the incidence angles ($\leq 2.5^\circ$) at the beamline optics introduce negligible changes in the beam's polarization. At each energy, there is good agreement between measurement and theory out to large ψ values. This confirms that the beamline optics are well aligned. A more rapid fall in P_L with ψ is evident at higher energy as expected.

An upper limit to the degree of unpolarized radiation can be estimated from the experimental data alone. This is accomplished by determining the most linearly polarized portion of the beam measured and assuming that the remaining portion is unpolarized. (Carr 1995) Assuming that this degree of unpolarized radiation is constant with ψ allows a lower limit to P_C to be determined, even in the presence of possible

unpolarized radiation. However, the theoretical calculations for a perfectly polarized source yield P_L values in excellent agreement with the measured values. This indicates that the remaining radiation is not unpolarized, but rather is the small amount of circularly polarized radiation entering the narrow slit due to its non-zero size. Thus, in this experimental determination of P_C from equation (D12), it is assumed that the amount of unpolarized radiation is zero. The true amount of unpolarized radiation present is less than the uncertainty in the measurement. With the narrow slit at $\psi = 0$ mrad, the theoretical value for P_L is 0.9993 and 0.991 for 367 and 722 eV, respectively.

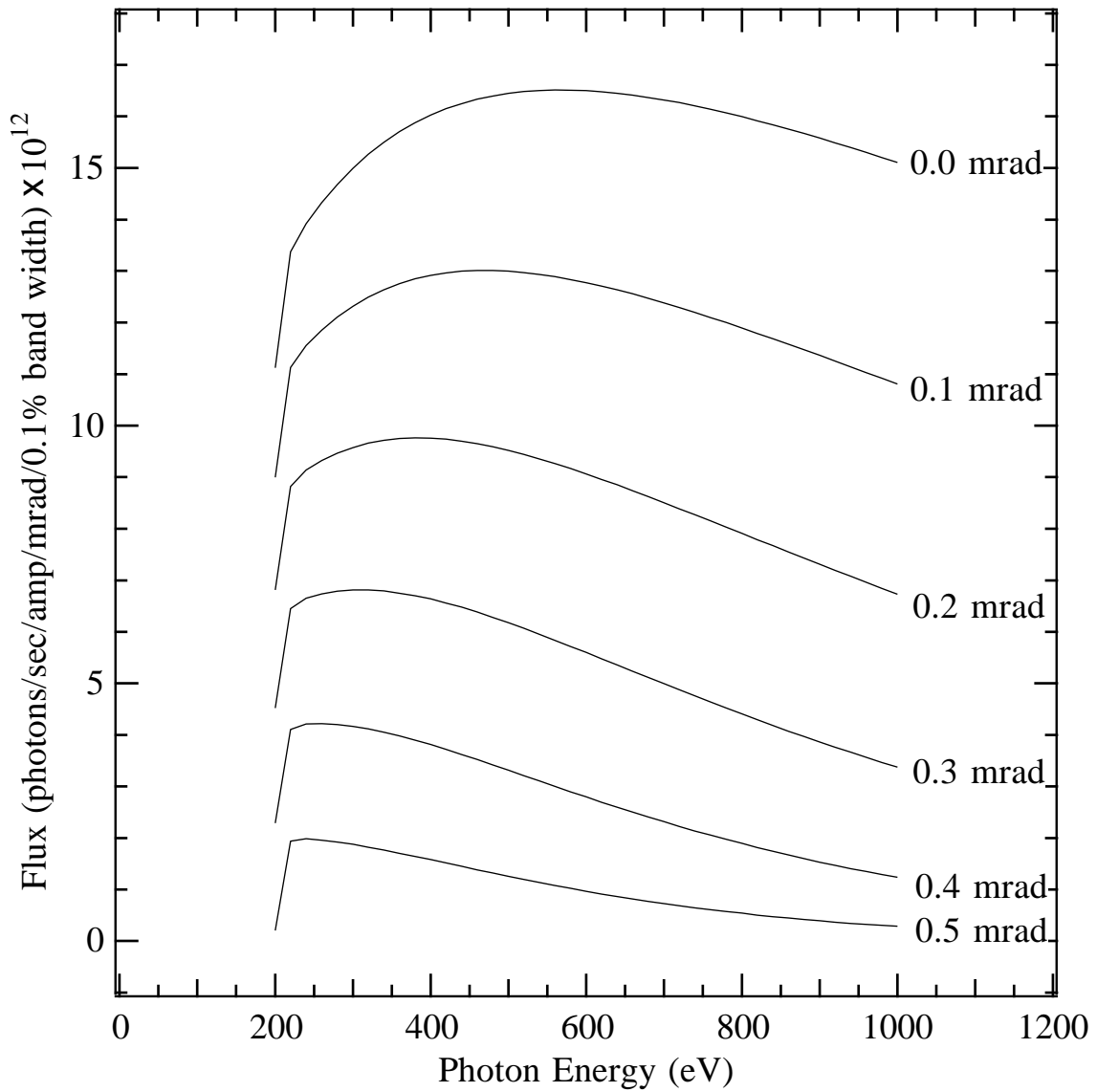
Polarization and flux response to blocking the beam from above and below the horizon using the larger semi-aperture were investigated. Figures D6a and D6b show P_L , P_C , and the fractional flux measured at 367 eV and 722 eV, respectively, as a function of the semi-aperture position in the beam. For $\psi > 0$, the semi-aperture blocks the beam below the horizon; for $\psi < 0$, the semi-aperture blocks the beam above the horizon. Calculations were completed over an angular aperture roughly corresponding to that measured. An upper ψ limit of 0.5 and 0.6 mrad for 367 eV and 722 eV was assumed, respectively. At lower photon energies, the changing focal position of the spherical grating overfilled M3, causing it to act as an effective aperture. The flux data are the fraction of flux passing through the aperture normalized to the total flux if the aperture were positioned to pass the entire beam. Thus, the fractional flux has a value of 0.5 at $\psi = 0$ mrad.

The measured quantities are in generally good agreement with the theoretical calculations, although not as good as for the narrow slit. This is because the narrow slit has precisely determined edges defining a beam which entirely enters the polarimeter entrance pinhole. For the semi-aperture, the high-angle limit is less well known and a smaller fraction of the wider beam actually enters the polarimeter. At 367 eV (figure D6a), the measured fractional flux falls more rapidly than that calculated. This results because radiation reflected from the ends of the overfilled M3 are not within the phase space acceptance of the polarimeter. Such a loss of intensity for off-axis rays systematically affects polarimetry results. This causes an increased P_L and decreased P_C as compared to calculations which ignore such effects. This systematic departure of measured results from calculated results is evident in figure D6a; a similar departure is evident at high positive ψ at 722 eV (figure D6b).

The values of P_L and P_C in figures D6a and D6b at $\psi = 0$ mrad equal those measured for a wide open aperture passing the entire vertical fan. Thus, radiation from different parts of the vertical fan add incoherently at the experiment, as expected. This results in a beam with a significant degree of linear as well as both left and right circularly polarized components. Experimenters should be aware of the presence of these different polarization components when accepting a wide vertical aperture.

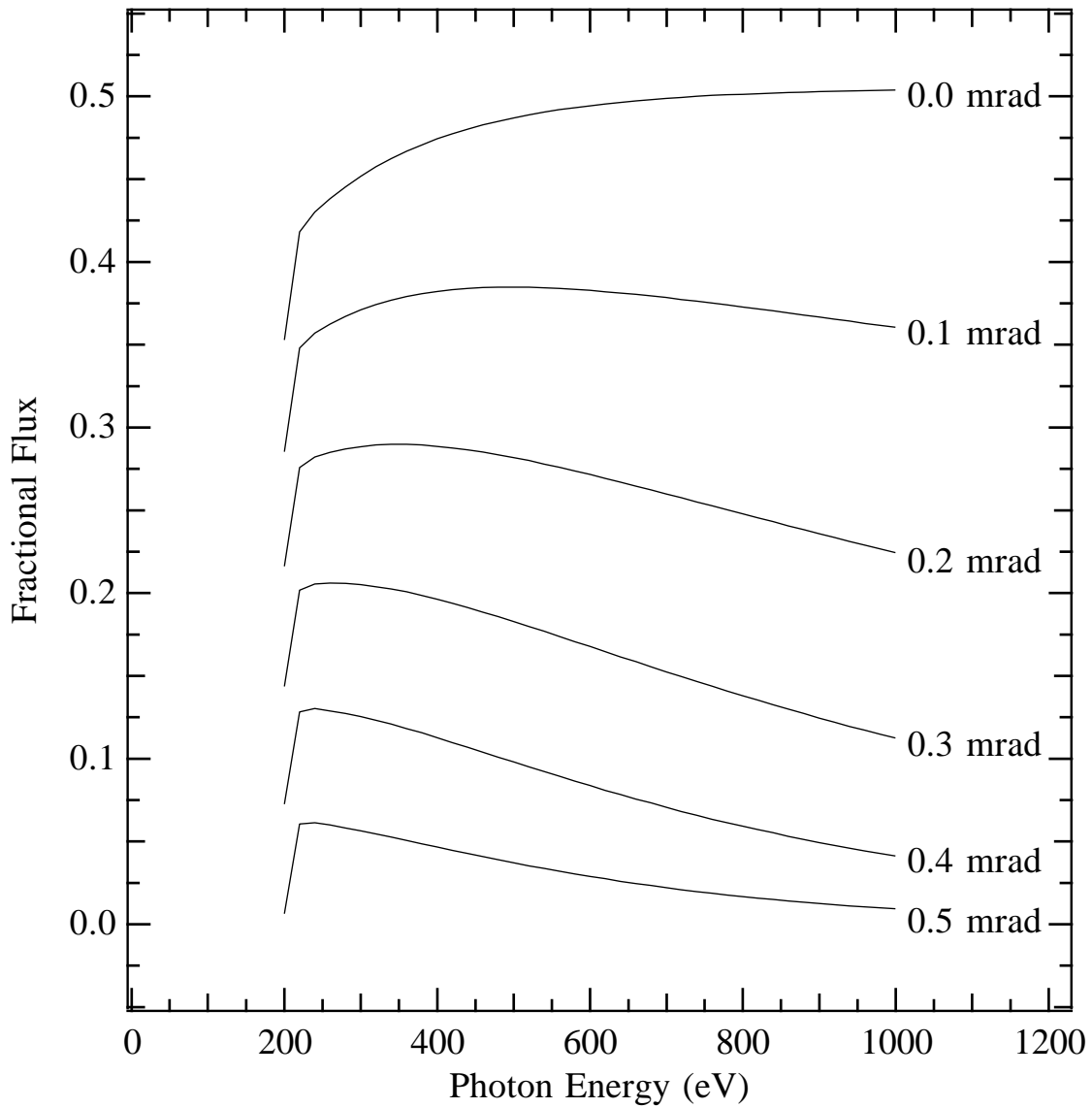
The semi-aperture data allowed the investigation and optimization of the merit function described by equation D8. Using P_C and the fractional flux from figures D6a and D6b, the merit function was calculated for each semi-aperture position. These experimentally determined results are plotted along with the theoretical values for 367 eV and 722 eV in figures D7a and D7b, respectively. A shallow minimum at $\psi = 0$ mrad is predicted but does not appear to be observed experimentally. The systematic departure of measured results from calculated results mentioned above cause the measured merit function to fall more rapidly with ψ than predicted. The merit function is optimized with the semi-

aperture at or just beyond $\psi = 0$ mrad. If this merit function overrides other experimental considerations, experiments using left or right circular polarization are best illuminated with only roughly a factor of 2 loss in total intensity. For some experiments, a high value of P_C may be of greater value than this merit function, in which case a more restricted off-axis vertical aperture may be selected.



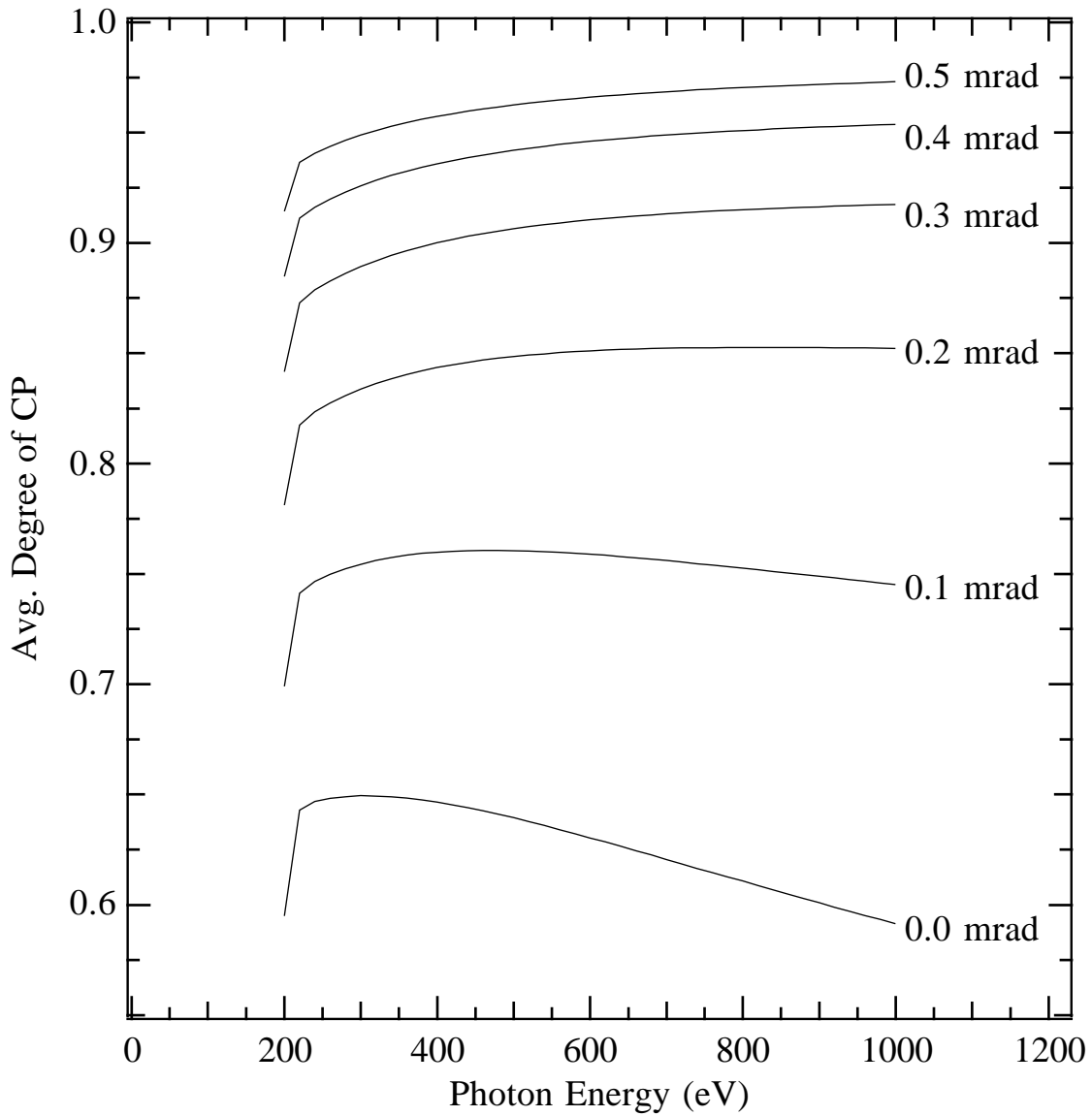
Total calculated flux from equation (D1) considering a grating line density of 600 lines/mm , a fixed included angle of 174° , and operated in the $m=+1$ diffraction order.

Figure D1



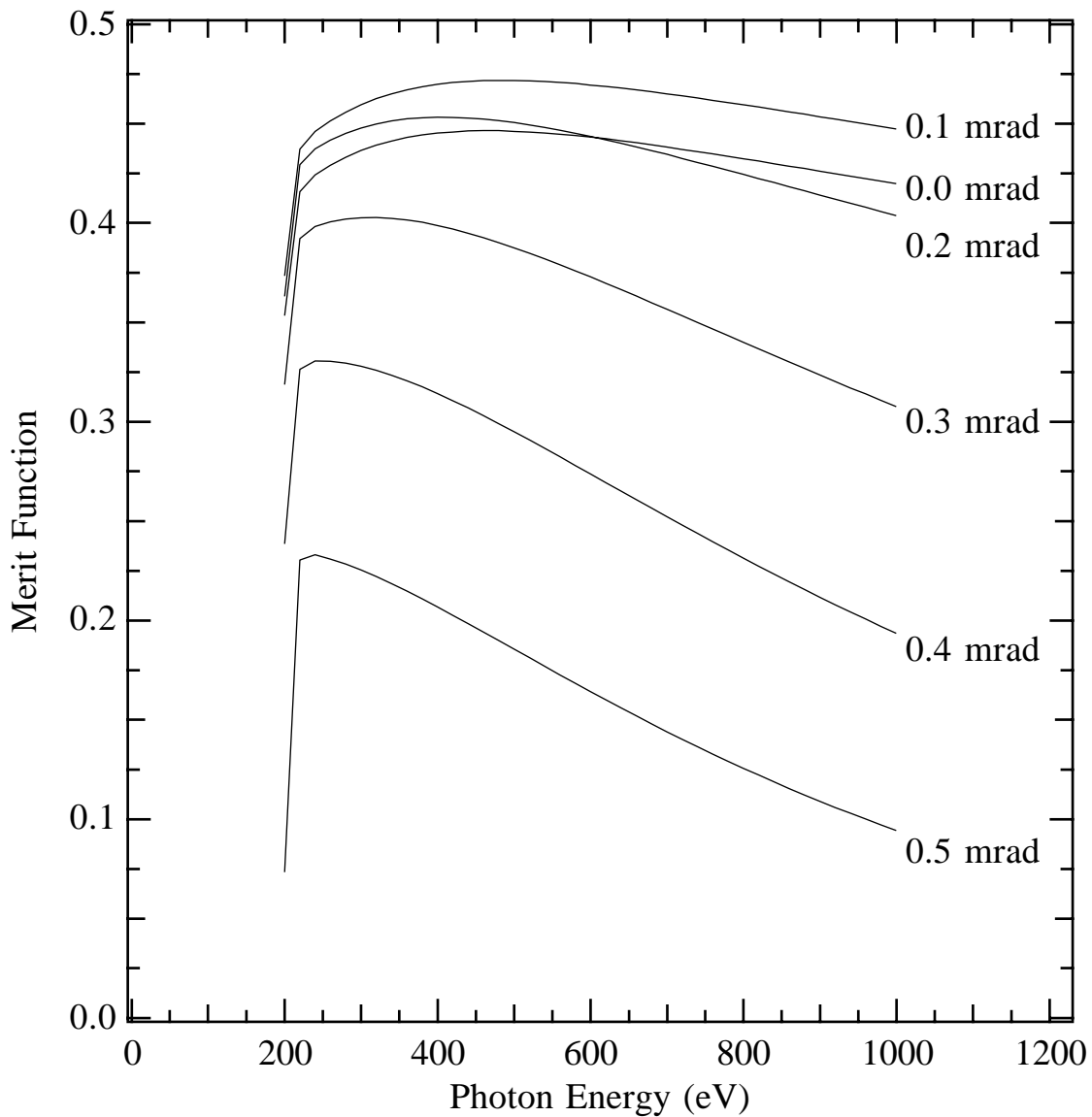
Calculated fraction of the total emitted flux accepted by an aperture defined by a lower value given by a central stop while the upper value is given by either the aperture of the horizontally deflecting mirror or the aperture of the grating. The half-apertures of the central stop are shown ranging from 0.0 to 0.5 mrad. Larger central stop sizes cause a significant flux reduction, especially at high energies.

Figure D2



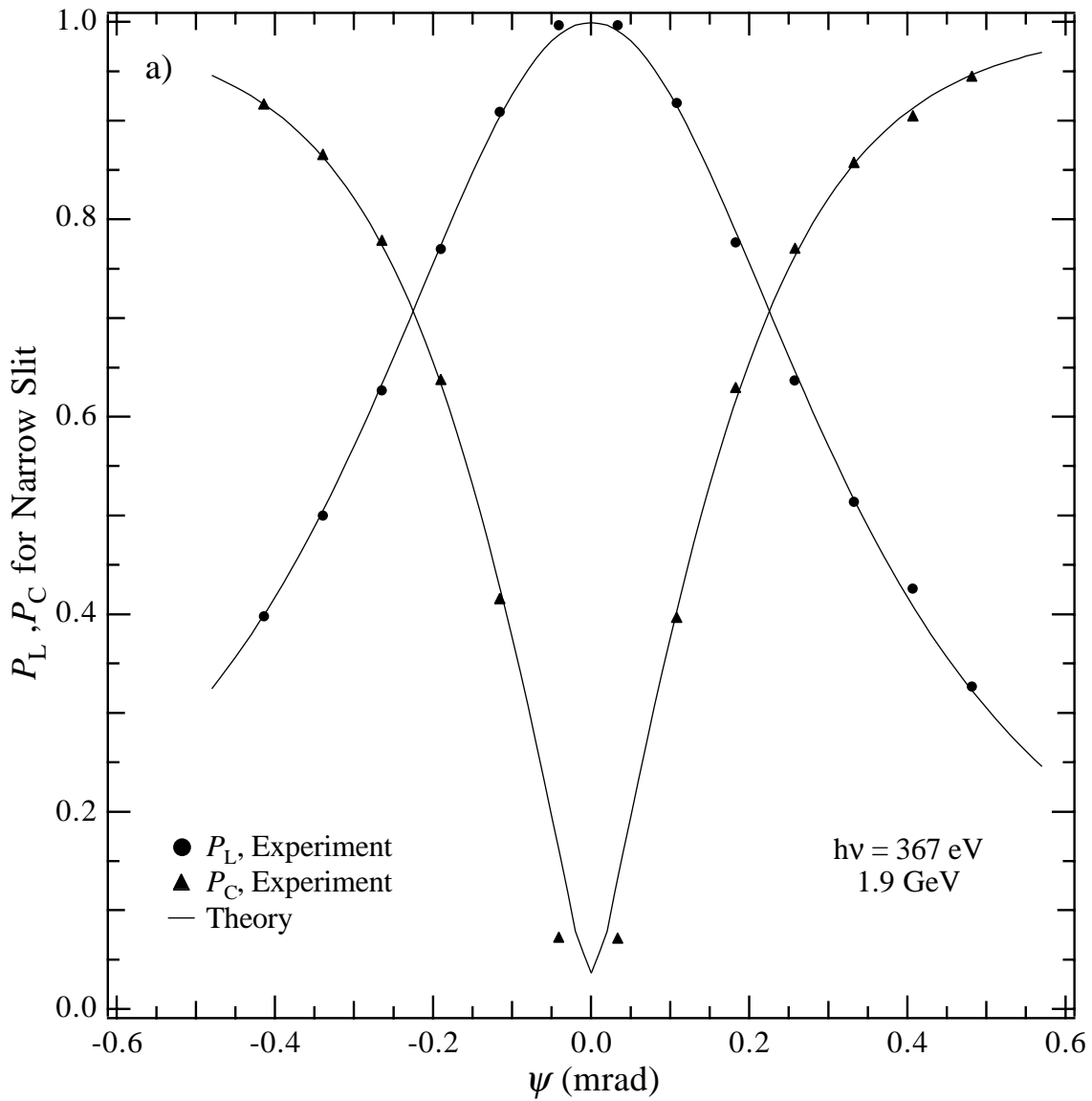
Calculated average degree of circular polarization for an aperture defined by a lower value given by a central stop while the upper value is given by either the aperture of the horizontally deflecting mirror or the aperture of the grating. The half-apertures of the central stop are shown ranging from 0.0 to 0.5 mrad. For the largest stop size, the degree of circular polarization is greater than 0.9. Even with no stop, it is typically greater than 0.6 throughout the energy range.

Figure D3



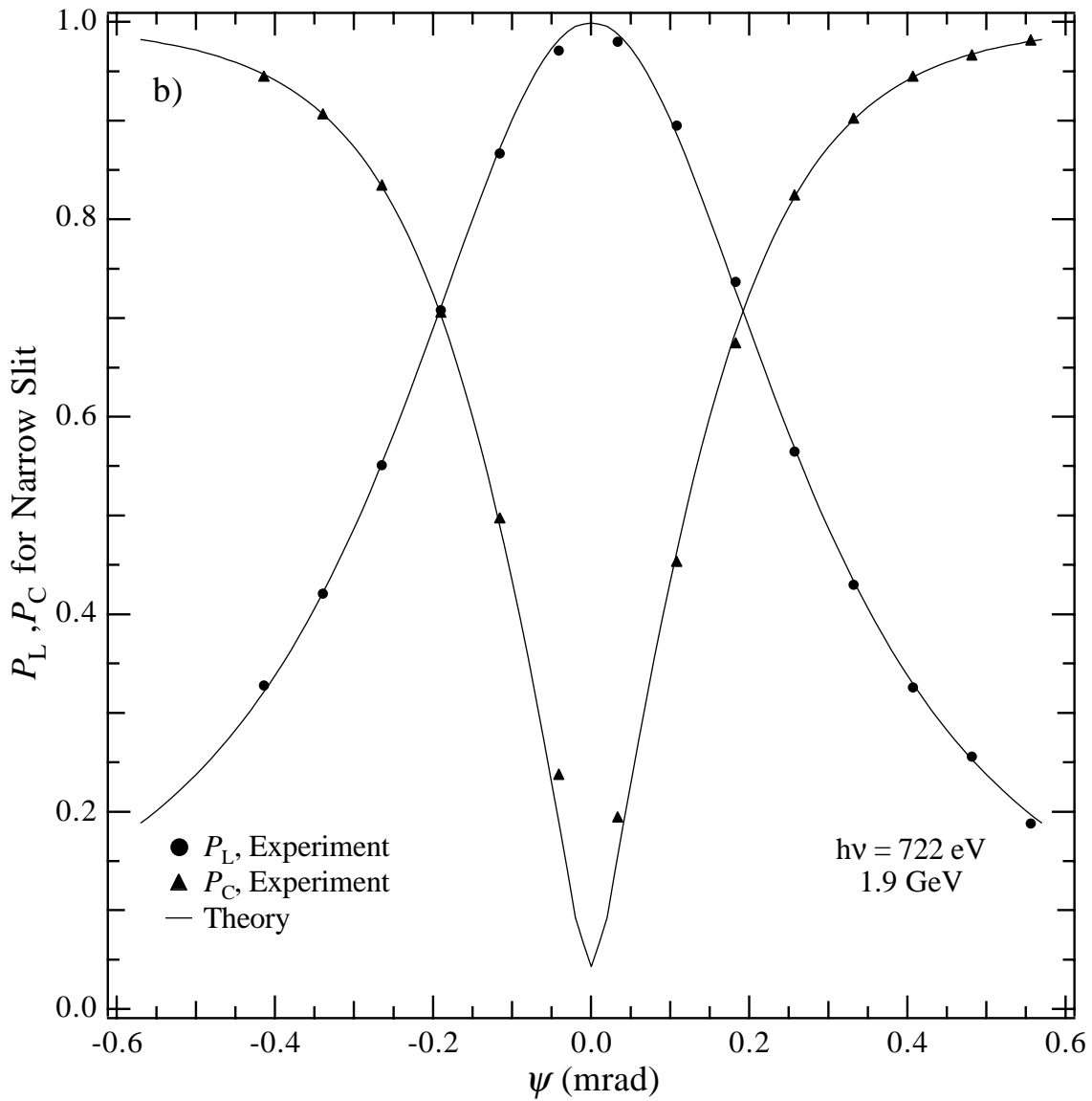
Calculated merit function for an aperture defined by a lower value given by a central stop while the upper value is given by either the aperture of the horizontally deflecting mirror or the aperture of the grating. The half-apertures of the central stop are shown ranging from 0.0 to 0.5 mrad. The merit function weights the average degree of circular polarization with the fraction of the total emitted flux actually accepted. The merit functions over the half-aperture sizes 0.0, 0.1, and 0.2 mrad are within 10% of each other over the entire energy range. This insensitivity is caused by the balance of decreasing flux and increasing degree of circular polarization.

Figure D4



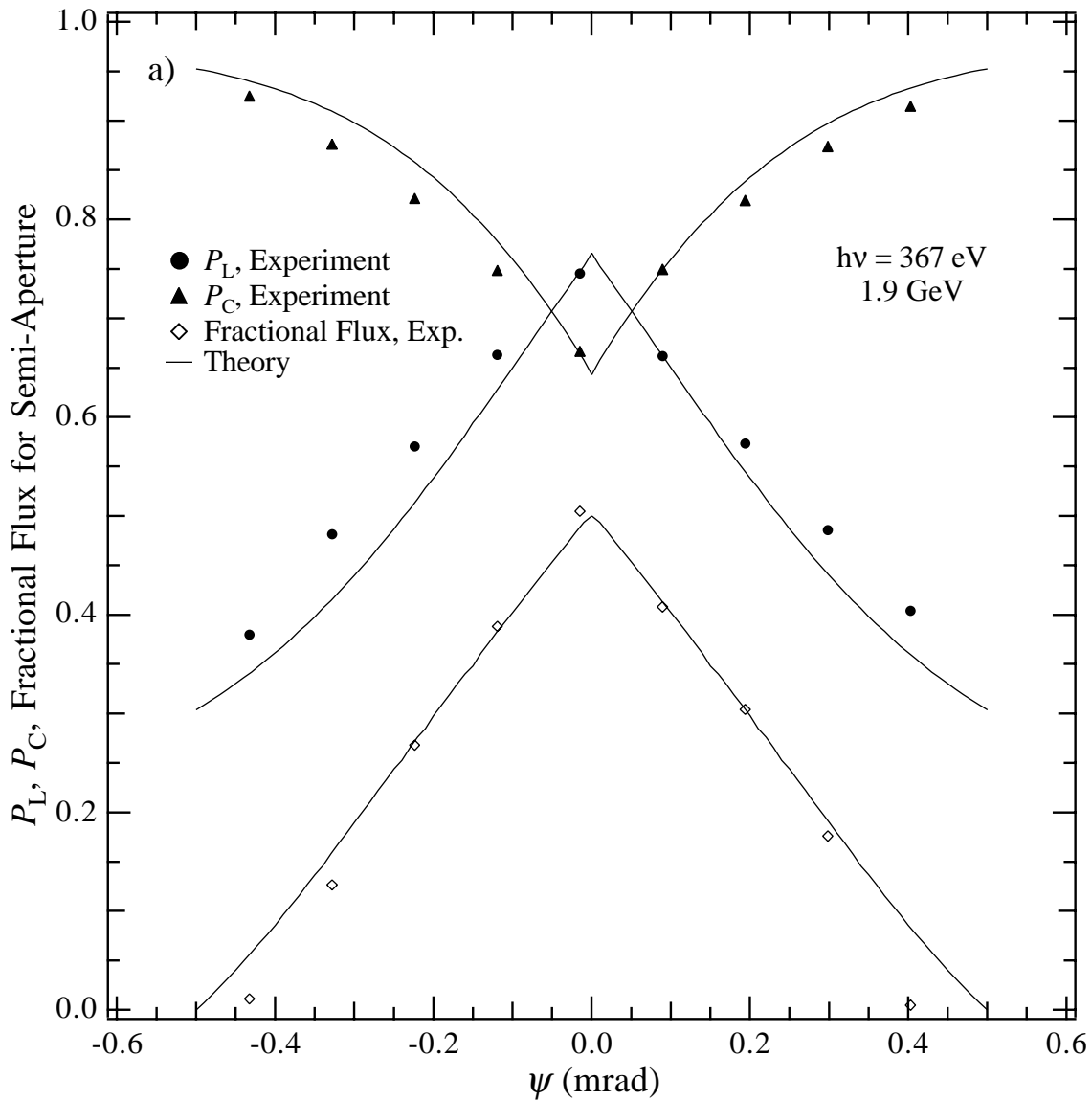
The degree of linear (P_L) and circular (P_C) polarization as the narrow slit (0.037 mrad) was stepped across the vertical opening angle for 367 eV photon energy. Symbols represent the experimental values; experimental P_C values were obtained by assuming that the amount of unpolarized radiation was zero. Lines represent the calculated values. Even with the slit at $\psi = 0$ mrad, there is a small amount of circular polarization transmitted due to the non-zero slit width.

Figure D5a



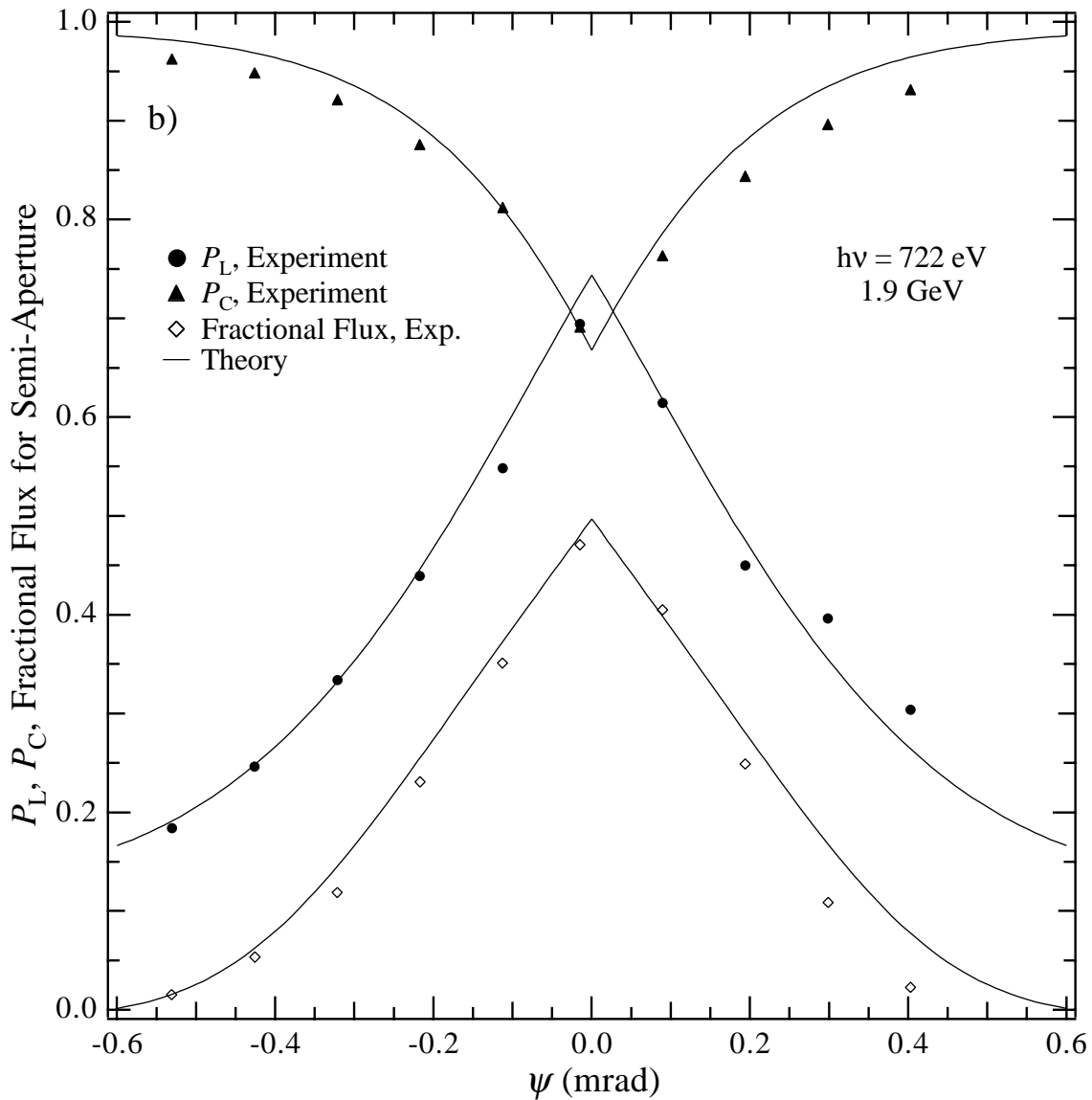
The degree of linear (P_L) and circular (P_C) polarization as the narrow slit (0.037 mrad) was stepped across the vertical opening angle for 722 eV photon energy. Symbols represent the experimental values; experimental P_C values were obtained by assuming that the amount of unpolarized radiation was zero. Lines represent the calculated values. Even with the slit at $\psi = 0$ mrad, there is a small amount of circular polarization transmitted due to the non-zero slit width.

Figure D5b



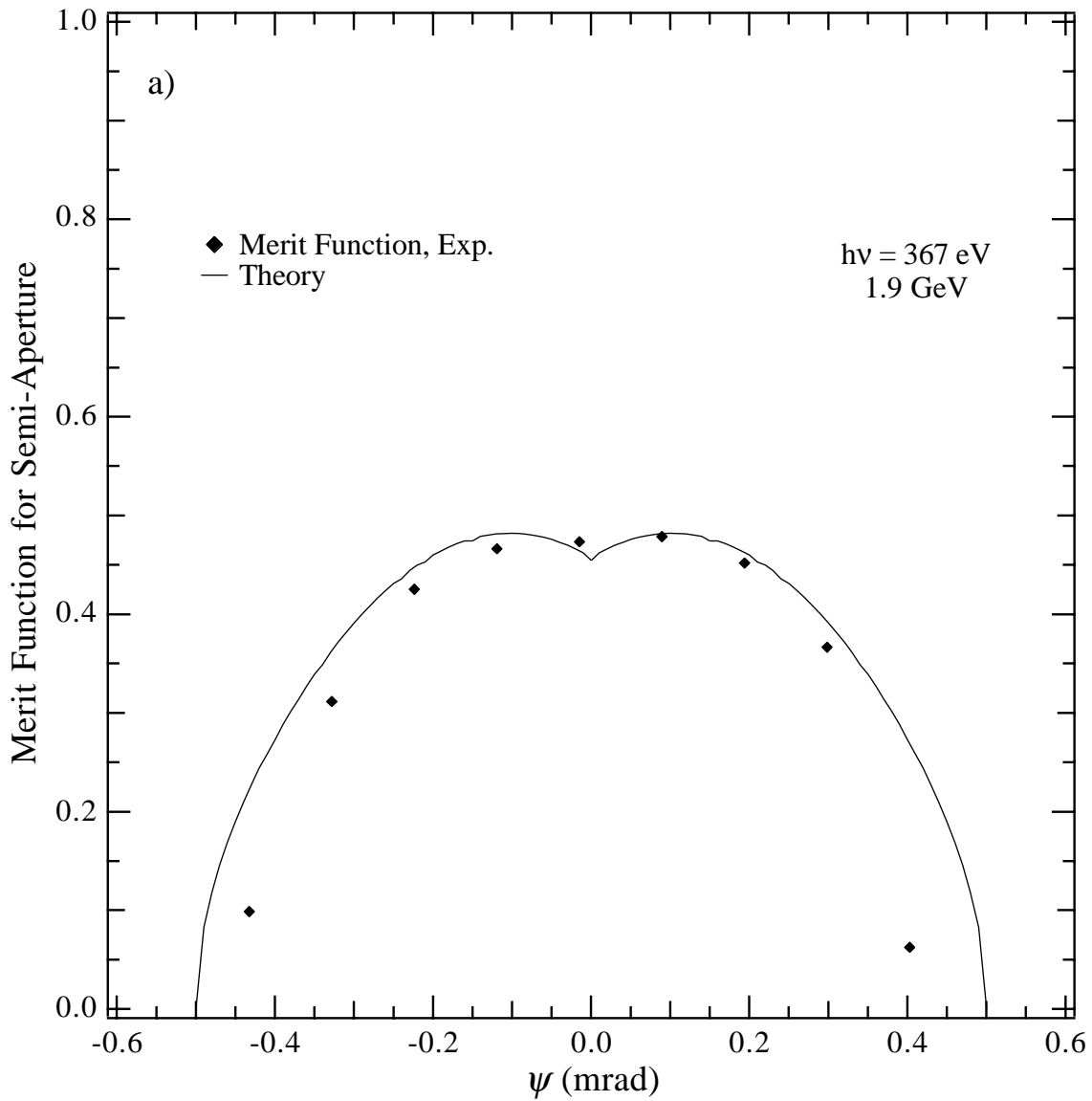
The degree of linear (P_L) and circular (P_C) polarization and the fractional flux as the wide semi-aperture was stepped across the vertical opening angle for 367 eV photon energy. For $\psi > 0$, the semi-aperture blocks the beam below the horizon; for $\psi < 0$, the semi-aperture blocks the beam above the horizon. Symbols represent the experimental values; experimental P_C values were obtained by assuming that the amount of unpolarized radiation was zero. Lines represent the calculated values. With the semi-aperture removed to transmit the entire beam, the measured P_L and P_C values equal those measured with the aperture edge at $\psi = 0$ mrad.

Figure D6a



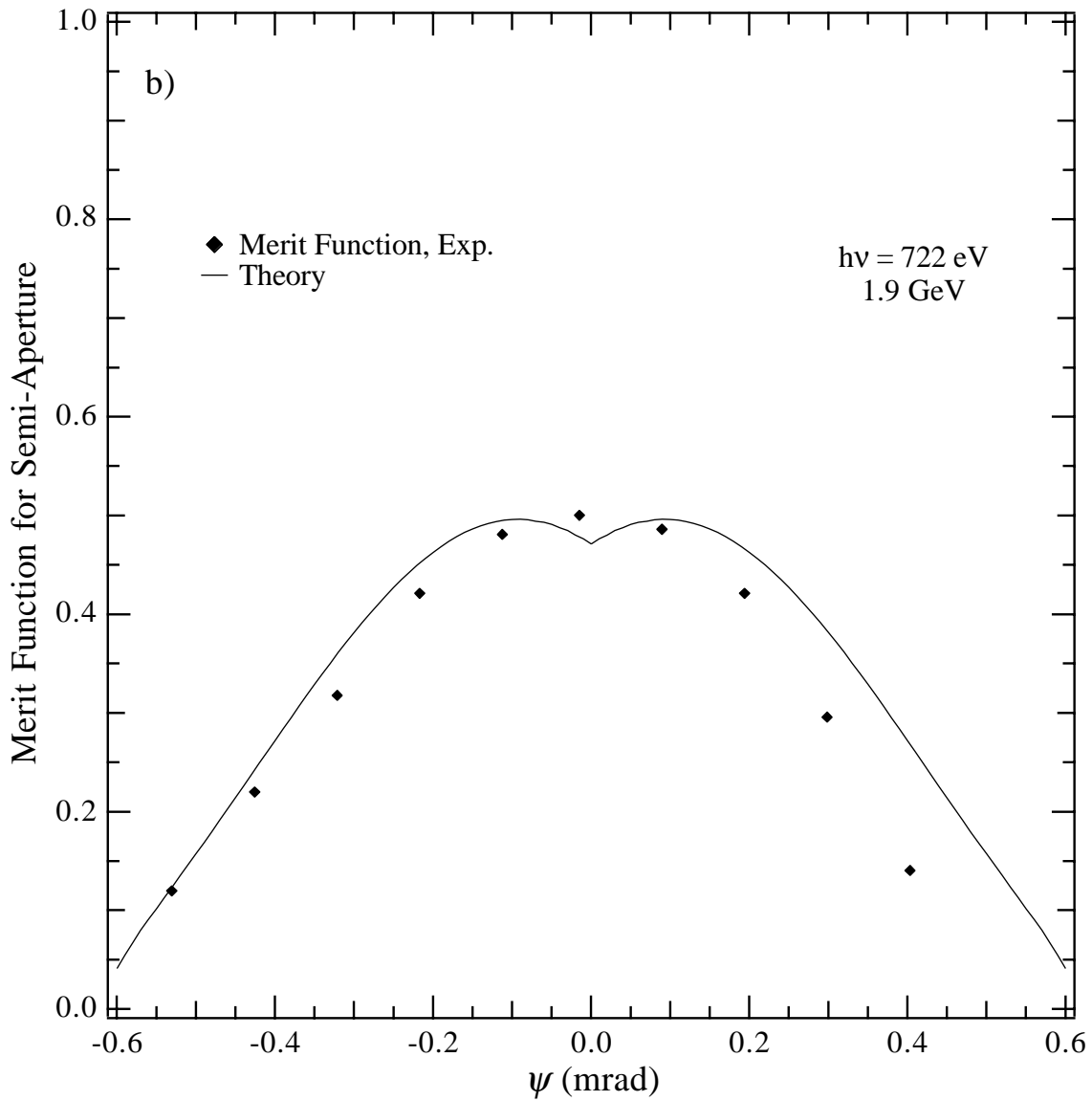
The degree of linear (P_L) and circular (P_C) polarization and the fractional flux as the wide semi-aperture was stepped across the vertical opening angle for 722 eV photon energy. For $\psi > 0$, the semi-aperture blocks the beam below the horizon; for $\psi < 0$, the semi-aperture blocks the beam above the horizon. Symbols represent the experimental values; experimental P_C values were obtained by assuming that the amount of unpolarized radiation was zero. Lines represent the calculated values. With the semi-aperture removed to transmit the entire beam, the measured P_L and P_C values equal those measured with the aperture edge at $\psi = 0$ mrad.

Figure D6b



The merit function given by equation (D8) as the semi-aperture was stepped across the vertical opening for 367 eV photon energy. Symbols represent the experimental values. Lines represent the calculated values. The merit function is optimized with the semi-aperture blocking roughly half of the total intensity.

Figure D7a



The merit function given by equation (D8) as the semi-aperture was stepped across the vertical opening for 722 eV photon energy. Symbols represent the experimental values. Lines represent the calculated values. The merit function is optimized with the semi-aperture blocking roughly half of the total intensity.

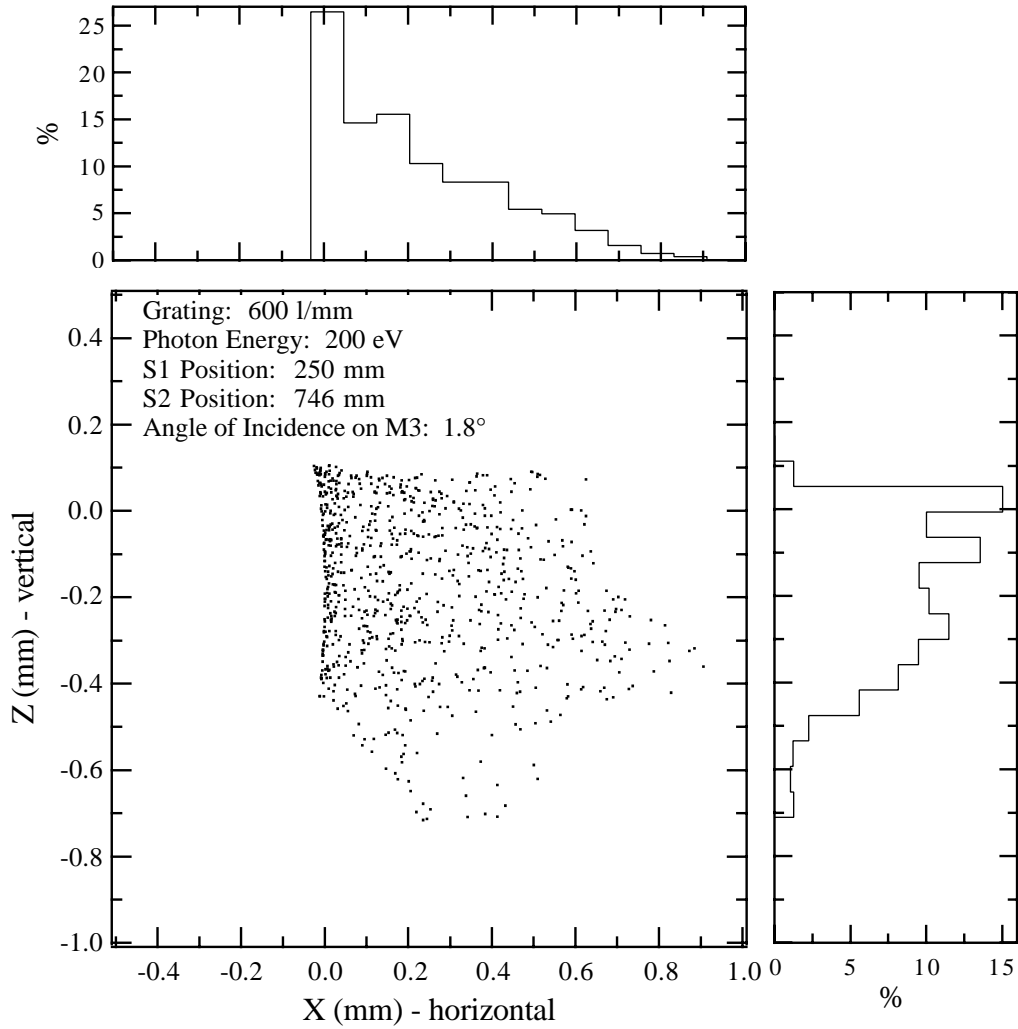
Figure D7b

Ray Tracing Calculations

Using the ray-tracing program SHADOW, calculations were performed to illustrate how the photon beam focus at the endstation depends on the exit slit position and the photon energy. Figure 2 in the main text shows the optical geometry. The mirror dimensions and geometries are listed in Appendix A.

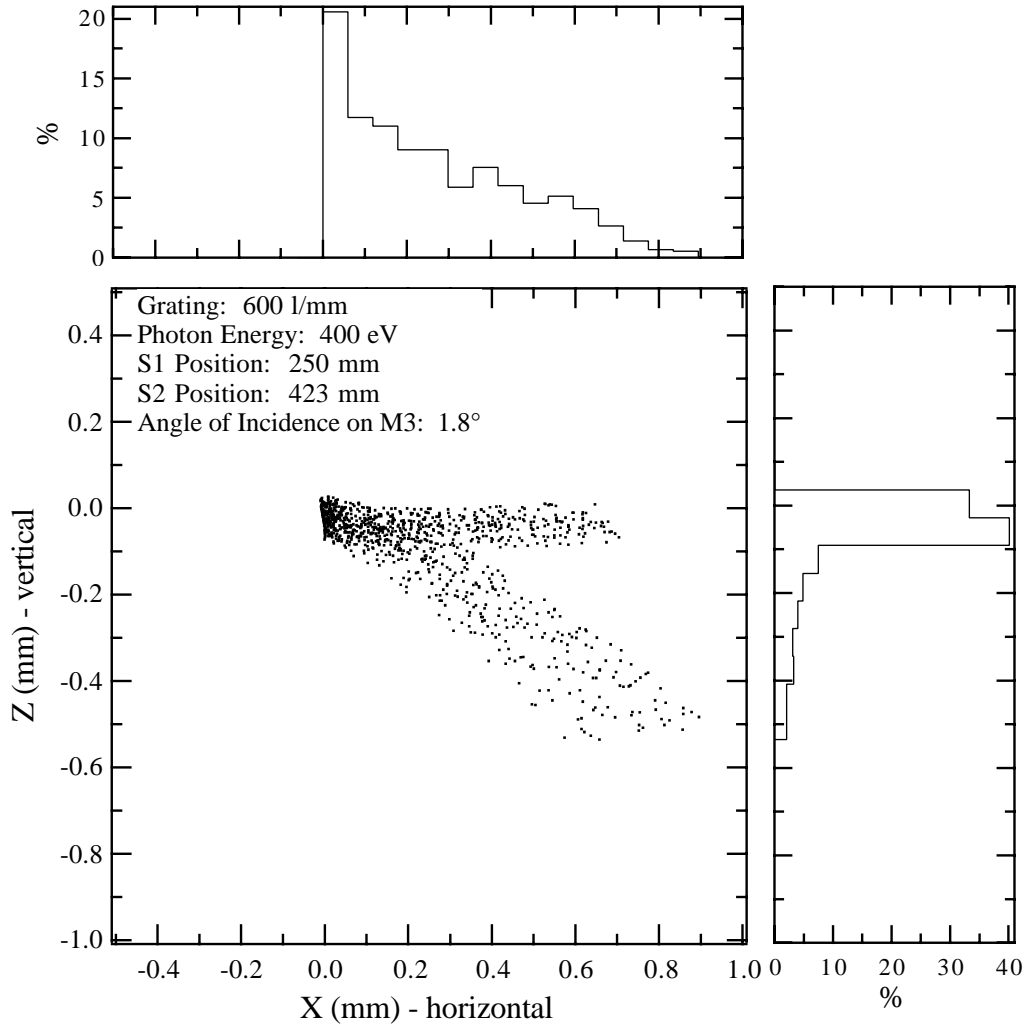
For the calculation results presented here, the angle of incidence on the refocusing mirror, M3, was 1.8° . The M3 meridian radius was fixed at 87.0 m to vertically focus the beam 2.17 m downstream of M3 when the exit slit, S2, is at 423 mm. This position satisfies the focus condition at 400 eV when the entrance slit, S1, is at 250 mm. The slit positions noted here are in units of millimeters as would be set by the user. To horizontally focus the beam 2.17 m downstream of M3, the sagittal M3 radius was fixed at 0.10 m because the M1 horizontal focus is 1.47 m downstream of the grating center (6.33 m upstream of the M3 center). Refer to Appendices B and C for an explanation of the foci calculations and the focus condition.

Using the 600 lines/mm grating, calculations were performed at three different energies. S1 was fixed at 250 mm for all of the calculations; this is the M2 vertical focus. S2 was set to satisfy the focus condition for each photon energy. At the lower limit of the grating, 200 eV, S2 was at 746 mm (see figure E1). As stated above, the conditions for 400 eV were used to fix the M3 geometry and S2 was at 423 mm (see figure E2). The exit slit maximum travel, 1000 mm, was reached at 740 eV (see figure E3). Comparing figures E1, E2, and E3, one can see that the beam comes into and out of focus if the M3 geometry and orientation is fixed. However, this effect turns out to be negligible when doing photoemission experiments.



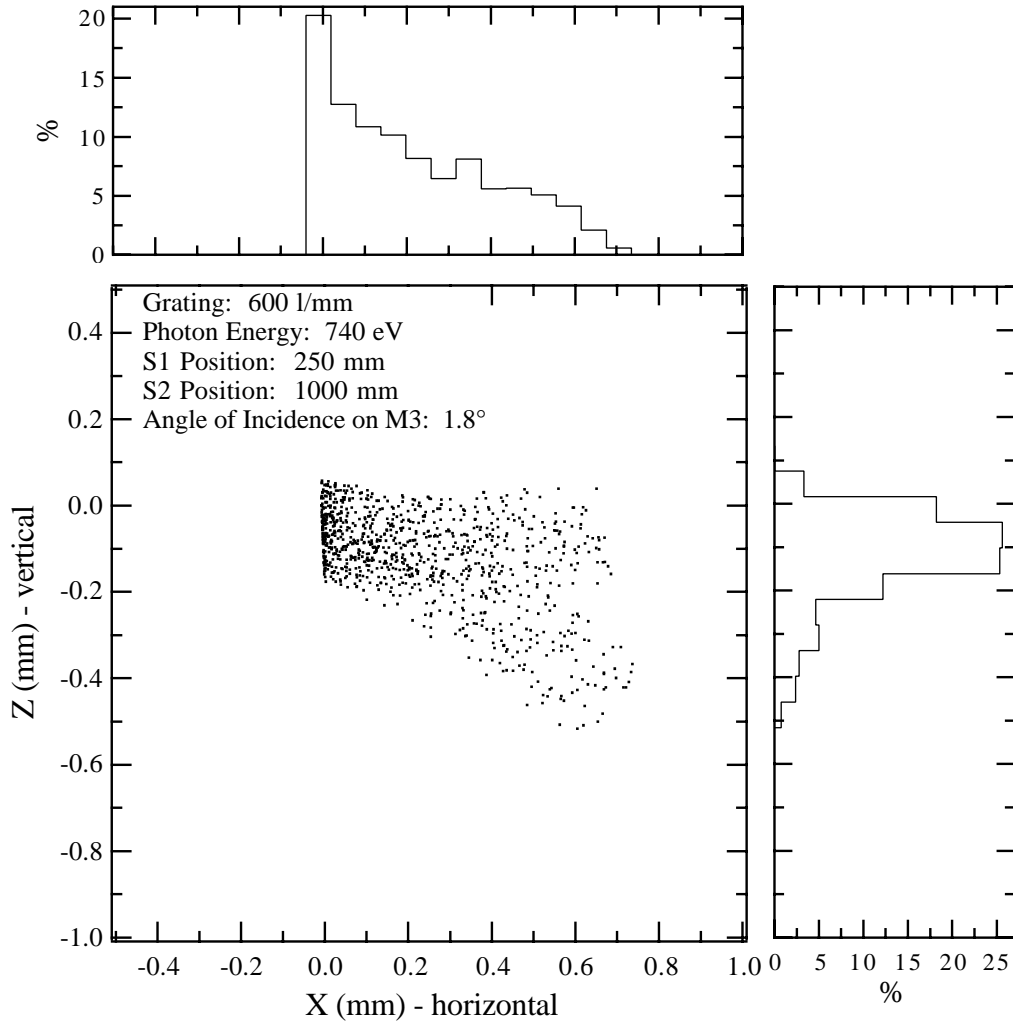
Focal spot for $h\nu = 200$ eV using the 600 $\frac{\text{lines}}{\text{mm}}$ grating. The slit positions satisfy the focus condition. The angle of incidence on M3 was 1.8°. As shown by the histograms, the majority of the flux falls within a beamsize $\sim 0.5 \times 0.4$ mm.

Figure E1



Focal spot for $h\nu = 400$ eV using the 600 $\frac{\text{lines}}{\text{mm}}$ grating. The slit positions satisfy the focus condition. The angle of incidence on M3 was 1.8°. As shown by the histograms, the majority of the flux falls within a beamsize $\sim 0.5 \times 0.2$ mm.

Figure E2



Focal spot for $h\nu = 740$ eV using the 600 $\frac{\text{lines}}{\text{mm}}$ grating. The slit positions satisfy the focus condition. The angle of incidence on M3 was 1.8°. As shown by the histograms, the majority of the flux falls within a beamsize $\sim 0.5 \times 0.3$ mm.

Figure E3

BEAMLINE ATTRIBUTES

Circular Polarization

Bending magnet synchrotron radiation is linearly polarized with the polarization vector in the orbit plane. Viewing at any angle other than in the orbit plane, however, the perpendicular component of the polarization vector becomes non-zero. The net polarization is thus elliptical at any viewing angle other than in the orbit plane. The helicity of the elliptically polarized light changes when changing the viewing angle from above to below the orbit plane. Additionally, the degree of circular polarization increases as the out of plane viewing angle increases. Of course, the flux decreases for these larger angles. The optimum balance between circular polarization and flux within the limitations imposed by the beamline geometry must be determined before carrying out experiments using circularly polarized light. (Green 1977; Padmore 1993)

A water-cooled aperture is installed upstream of the vertically deflecting mirror which can be positioned with 1 μm resolution to select the beam centroid for linearly polarized light. Alternatively, the aperture can be positioned above or below the beam center to select circularly or elliptically polarized light.

A 0.5 mm slit below the selection aperture is used to determine the beam centroid; the degree of linear polarization through this slit was measured to be 0.99 at the endstation. (Kortright 1995; Kortright 1996) The degree of circular polarization as measured at the endstation is over 0.8 at 700 eV with the circular polarization flux $\geq 30\%$ of the total flux. (Kortright 1996) .

Photodiodes

A photodiode is installed downstream from each optical component to aid alignment and storage ring diagnostics. These are electrically isolated to allow for photocurrent measurements and/or coated with phosphor for viewing the beam. The parts used to collect photocurrent signals expose a clean gold surface to the beam. Thus, absolute flux calculations can be performed.

I-zero

Directly downstream of M3 are a gold grid and a copper grid (>85% transmission). Evaporators for each metal are maintained so that a fresh layer can be deposited on the respective grid and a clean I-zero signal can be collected. These grids are electrically isolated and the I-zero photocurrent can be measured directly. A potential may be applied to an electrically isolated wire loop surrounding the face of the grids to collect all photoelectrons and thus improve the stability and accuracy of the measured photocurrent. Alternatively, one can measure total yield by using a channeltron positioned 90° to the beam.

Rotating Platform Endstation

Mounted on a rotating platform are two different endstations. The platform rotates manually through 60° in <5 minutes allowing the beam to be directed to either endstation without breaking the vacuum. The two halves of the platform are vibrationally decoupled from one another to allow assembly of one endstation while the other takes beam. The rotation stops have been designed to align the chambers upon successive rotations. For

structural stability, the chambers are bolted through the platform to pods secured to the floor. This removes the 'drum-head' effect of the large platform.

Permanently mounted at station one is the Advanced Photoelectron Spectrometer/Diffractometer (APESD) (*Ynzunza to be published*) with an angle resolving Scienta SES 200 hemispherical electron energy analyzer for doing a variety of surface science experiments. These include high resolution photoelectron diffraction (scanned angle and/or energy) and x-ray photoelectron spectroscopy (XPS) of surfaces and interfaces. Additionally, magnetic circular dichroism (MCD) as well as x-ray total-reflection XPS studies are being performed at station one.

Mounted at station two is the Applied Materials Chamber (*Kellar to be published*) with a partial yield electron and fluorescence detector for near-edge x-ray absorption fine structure (NEXAFS) and MCD studies. An angle integrating electron energy analyzer is used for XPS studies. Alternately mounted at station two is the Angle-Resolved PhotoEmission Spectrometer (ARPES) with a movable electrostatic hemispherical electron energy analyzer (mean radius of 50 mm) used for studying surfaces and interfaces. (*Kevan 1980*) This system is mainly used for studying angle-resolved photoemission extended fine structure (ARPEFS - scanned energy photoelectron diffraction).

A third endstation is mounted upstream of M3. A deflecting mirror is used to direct the photon beam through the gas cell to the Fourier Transform Soft X-Ray (FTSX) spectrometer. (*Moler 1996*) The FTSX spectrometer will be used for ultra-high resolution spectroscopic studies of gas-phase core-levels from $h\nu = 40 - 120$ eV.

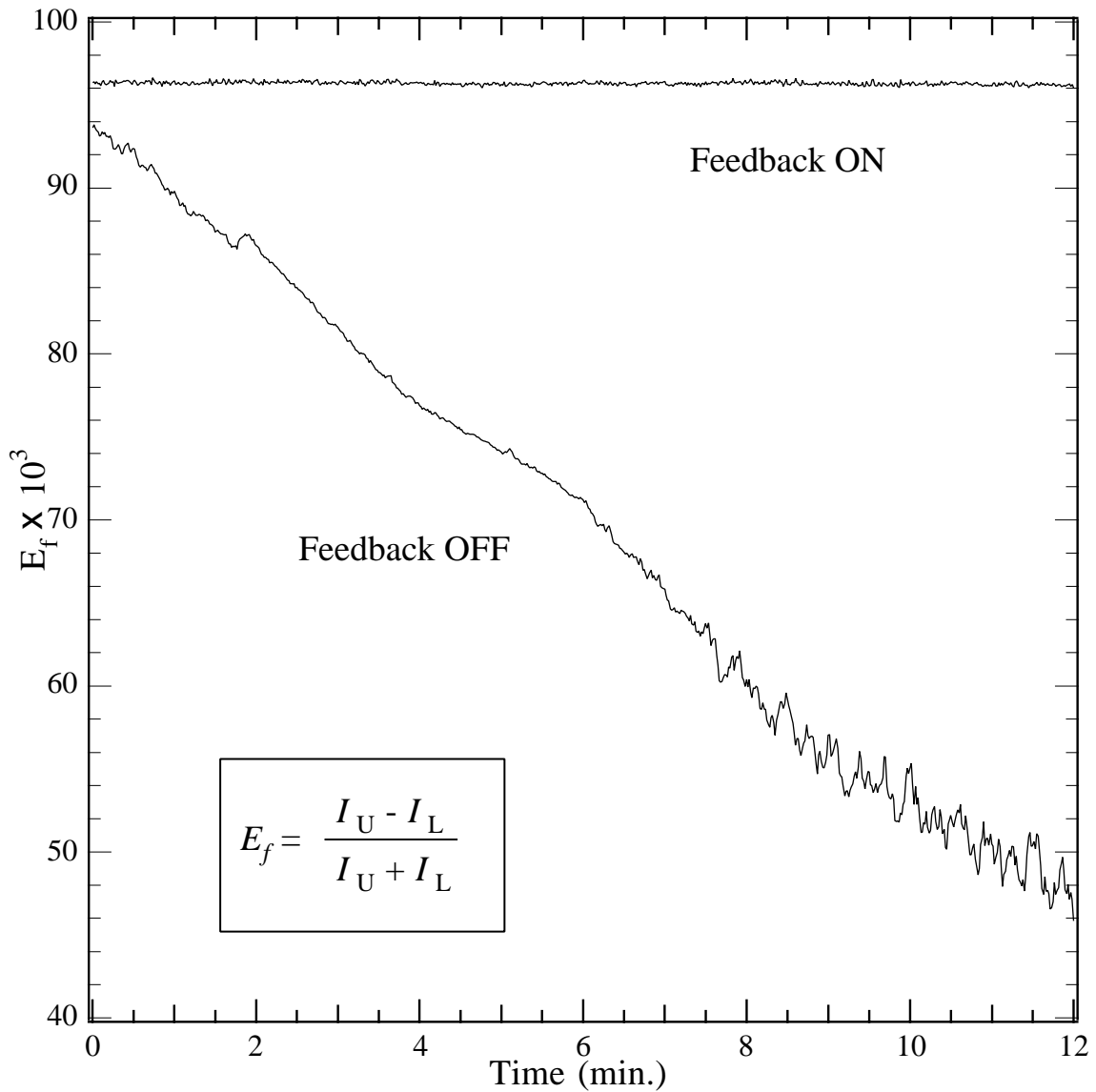
Active Feedback on M2 Pitch

A beam position locking system was developed to correct for photon beam fluctuations. The most notable cause has been temperature variations of the low conductivity water (LCW) which is used to cool the ALS magnets and some optics. LCW temperature must not vary more than ± 0.1 C° to maintain a stable photon beam.

The beamline is controlled by the Experimental Physics and Industrial Controls Systems (EPICS). The Proportional, Integral, and Derivative (PID) control algorithm in EPICS (*Anderson 1992*) is used for this beam position locking. The upper and lower S1 jaws are electrically isolated from each other and from ground. The photocurrent from each jaw is measured to determine the signal difference. This signal in conjunction with the PID logic is used to generate an error function, E_f ,

$$E_f = \frac{I_U - I_L}{I_U + I_L} \quad (1)$$

where I_U and I_L are the photocurrent signals from the upper and lower jaws, respectively. This error function is utilized to automatically adjust a piezoelectric drive that changes the M2 pitch. The feedback routinely operates at 10 Hz.



Error function used for the feedback loop as a function of time. Without the feedback loop in operation, the beam can drift causing the changes in the photocurrent collected from each jaw. However, when in operation, the feedback loop effectively locks the beam position thus stabilizing the flux at the endstation to better than 1%.

Bibliography

- Anderson, J.B. and Kraimer, M.R. (1992). *EPICS IOC Reference Manual*, Los Alamos National Laboratory.
- Carr, R., Kortright, J.B., Rice, M. and Lidia, S. (1995). "Polarimeter Reference." Rev. Sci. Instrum. **66**: 1862.
- Collett, E. (1993). Polarized Light. New York, Marcel Dekker, Inc.
- Fonzo, S.D., Jark, W., Schafers, F., Petersen, H., et al. (1994). "Polarimeter Reference." Appl. Optics **33**: 2624.
- Green, K. (1977). *Proposal for a National Synchrotron Light Source*, Brookhaven National Laboratory.
- Heimann, P.A., Senf, F., McKinney, W., Howells, M., et al. (1990). "High Resolution Results from the LBL 55-Meter SGM at SSRL Near the K-Edge of Carbon and Nitrogen." Physica Scripta **T31**: 127-130.
- Hogrefe, H., Howells, M.R. and Hoyer, E. (1986). "Application of Spherical Gratings in Synchrotron Radiation Spectroscopy." SPIE **733**: 274-285.
- Howells, M.R. (1995). *Bending Mechanisms*, Unpublished.
- Kellar, S.A., Hartman, N., Hussain, Z., Huff, W.R.A., et al. (to be published). "AMC Technical Report." .
- Kevan, S.D. (1980). *Ph.D. Thesis*, The University of California, Berkeley.
- Kimura, H., Yamamoto, M., Yanagihara, M., Maehara, T., et al. (1992). "Polarimeter Reference." Rev. Sci. Instrum. **63**: 1379.
- Kirz, J., Attwood, D.T., Henke, B.L., Howells, M.R., et al. (1986). *X-Ray Data Booklet*, Center for X-Ray Optics, Lawrence Berkeley Laboratory.
- Kortright, J.B., Rice, M. and Franck, K.D. (1995). "Tunable Multilayer EUV/Soft X-ray Polarimeter." Rev. Sci. Instrum. **66(2)**: 1567-1569.
- Kortright, J.B., Rice, M.A., Hussain, Z., Padmore, H.A., et al. (1996). "Polarization Measurement and Vertical Aperture Optimization for Obtaining Circularly Polarized Bend-Magnet Radiation." Rev. Sci. Instrum. **67(9)**.
- Krumrey, M. and Tegeler, E. (1992). "Self-Calibration of Semiconductor Photodiodes in the Soft X-ray Region." Rev. Sci. Instrum. **63(1)**: 797-801.
- Kunz, C. (1979). Topics in Current Physics: Synchrotron Radiation, Techniques and Applications. Berlin, Springer-Verlag.
- McKinney, W.R., Howells, M.R., Lauritzen, T., Chin, J., et al. (1990). "The LBL 55-Meter Spherical Grating Monochromator at SSRL." Nucl. Instr. and Meth. **A291**: 221-224.

- Michette, A.G. (1986). Optical Systems for Soft X-Rays. New York, Plenum Press.
- Moler, E.J., Hussain, Z., Duarte, R.M. and Howells, M.R. (1996). "Design and Performance of a Soft X-ray Interferometer for Ultra-High Resolution Fourier Transform Spectroscopy." J. Electron Spectrosc. **80**: 309-312.
- Padmore, H.A., Hussain, Z. and Zheng, Y. (1993). *Selection of the Optimum Aperture Sizes for Circularly Polarized Spectroscopy on Beamline 9.3.2*, Lawrence Berkeley Laboratory.
- Petersen, H., Senf, F., Schäfers, F. and Bahrddt, J. (1995). "Monochromators for the Undulator U49 at the BESSY II Storage Ring." Rev. Sci. Instrum. **66(2)**: 1777-1779.
- Reich, T., Hussain, Z., Moler, E., Blackwell, M., et al. (1993). "High Resolution in the Soft X-ray Range from a Toroidal Grating Monochromator." Rev. Sci. Instrum. **64(9)**: 2552-2557.
- Ynzunza, R.X., Tober, E.D., Palomares, F.J., Wang, Z., et al. (to be published). "Scientia Instrumentation, 9.3.2.1." .